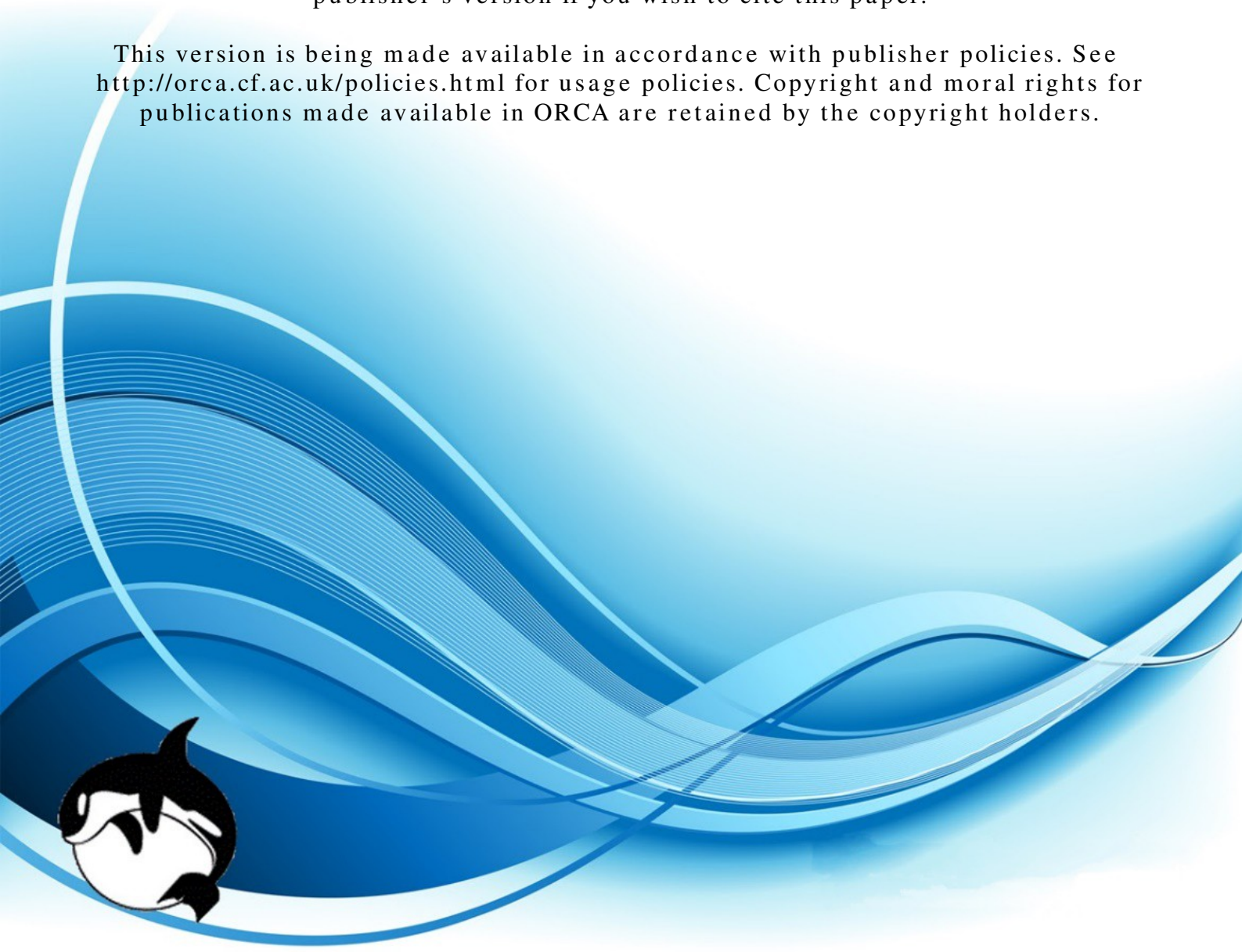

Uncertainties in remotely sensed precipitation data over Africa

INTERNATIONAL JOURNAL OF CLIMATOLOGY
RMetS Royal Meteorological Society

Uncertainties in remotely-sensed precipitation data over Africa

Journal:	*International Journal of Climatology*
Manuscript ID:	JOC-14-0463.R2
Wiley - Manuscript type:	Research Article
Date Submitted by the Author:	n/a
Complete List of Authors:	Awange, Joseph; Curtin University, Spatial Sciences Goncalves, Vagner; Hohai University, School of Earth Sciences and Engineering Forootan, Ehsan; Bonn University, Institute of Geodesy and Geoinformation Khandu, Khandu; Curtin University, Spatial Sciences Andam-Akorful, Samuel; Hohai University, Earth Science and Engineering; Kwame Nkrumah University of Science and Technology, Geomatic Engineering AGUTU, NATHAN; Curtin University, Spatial Sciences He, Xiufeng; Hohai University, School of Earth Sciences and Engineering,
Keywords:	modified three-cornered-hat (TCH), Multiple comparison proceedure , complex empirical orthogonal function (CEOF), Africa, Precipitation, Validation

Uncertainties in remotely-sensed precipitation data over Africa

J.L. Awange[a,*], V.G. Ferreira[b], E. Forootan[a,c], Khandu[a], S.A. Andam-Akorful[b,d], N.O. Agutu[a], X.F. He[b]

[a] *Western Australian Centre for Geodesy and The Institute for Geoscience Research, Curtin University, Perth, Australia*

[b] *School of Earth Sciences and Engineering, Hohai University, Nanjing, China*

[c] *Institute of Geodesy and Geoinformation, Bonn University, Bonn, Germany*

[d] *Department of Geomatic Engineering, Kwame Nkrumah University of Science and Technology, Kumasi, Ghana.*

Abstract

Quantifying the amount of precipitation and its uncertainty is a challenging task all over the world, particularly over the African continent, where rain gauge (RG) networks are poorly distributed. In recent decades, several satellite remote sensing (SRS)-based precipitation products have become available with reasonable spatial and temporal resolutions to be applied in hydrological and climate studies. However, uncertainties of these products over Africa are largely unknown. In this study, the generalized "three-cornered-hat" (TCH) method is applied to estimate uncertainties of gridded precipitation products over the entire African continent, without being dependent to the choice of a reference dataset. Six widely used SRS-based precipitation products (at monthly scales) were evaluated over the entire continent during the period of 2003-2010. The TCH results are further compared to those of the classical evaluation using the Global Precipitation Climatology Center (GPCC) over entire Africa, as well as to the RG observations over the Greater Horn of Africa (GHA). Overall, for the study period (2003–2010), the TCH results indicate that the RG-merged products contain smaller error amplitudes compared to the satellite-only products, consistent with the GPCC-based evaluation. A multiple comparison procedure ranking, which was applied based on signal-to-noise ratios (SNR)s, indicated that PERSIANN contains the highest SNR and thus suitable over most of Africa, followed by ARCv2, TRMM, CMORPH, TAMSAT and GSMaP. To extract the main spatio-temporal variability of rainfall over Africa, complex empirical orthogonal function technique

*Corresponding author
Email address: J.awange@curtin.edu.au (J.L. Awange)

was applied, from which the extracted patterns of GPCC, TRMM, PERSIANN, and ARCv2 were found to be similar but different from those of TAMSAT, CMORPH and GSMaP. Finally, the TCH and RG-based validation methods were found to provide similar evaluations for the SRS-only products (CMORPH and GSMaP) over GHA, with CMORPH emerging to be the most suitable product, consistent with previous studies.

Keywords: Africa, precipitation, validation, modified three-cornered-hat (TCH), complex empirical orthogonal function (CEOF), multiple comparison procedure (MCP)

1. Introduction

Precipitation is a key component of the global hydrological (water) cycle as its spatio-temporal distribution plays a significant role in balancing large-scale (e.g., basin-wide) water budget, as well as climate variability. Other than being the main source of renewable water resources, precipitation is also critical for socio-economic development of nations, especially African countries, which depend on rain-fed agriculture (*Dinku et al.*, 2007). In recent decades, most parts of the African continent have experienced high variability in precipitation that has led to recurrent drought and flood events in different countries (see, e.g., *Conway et al.*, 2009; *Tschakert et al.*, 2010; *Rojas et al.*, 2011; *Nicholson*, 2013; *Awange et al.*, 2014a; *Omondi et al.*, 2014). For example, in West Africa, and particularly the area below the Sahel region, anecdotal evidence from farmers suggests a forward shift in onset of rainy season over the past periods (*Giesen et al.*, 2010), while in the Great Horn of Africa (GHA), the number of extreme precipitation events has increased over the last few decades (*Omondi et al.*, 2014). Reliable and consistent estimates of precipitation information is, therefore, crucial for timely monitoring of water resources within the African continent.

The distribution of rain gauge (RG) networks within the African continent is, however, not adequate to reliably represent precipitation changes with respect to the continent's varying topography and climatic zones (e.g., *Hughes*, 2006; *Nicholson*, 2013). The RG observations might also not be readily available to the Global Telecommunication Systems (GTS) for onward usage in global data archives (*Nicholson et al.*, 2003a). Moreover, large-scale global and regional circulation processes (such as the El Niño Southern Oscillation – ENSO and inter-tropical convergence zone – ITCZ) have led to pronounced variability in precipitation at a wide range of spatial and temporal scales (see, e.g., *Awange et al.*, 2013, 2014b,c; *Omondi et al.*, 2012,

2013; *Forootan et al.*, 2014), thus making it more difficult to accurately measure precipitation changes. It is due to these deficiencies of *in-situ* RG observations that most meteorological and hydrological applications' needs are currently met by satellite remote sensing (SRS)-based precipitation products, although their reliability remains an issue (see, e.g., *Sawunyama and Hughes*, 2008; *Li et al.*, 2009).

A variety of SRS-based precipitation products from various institutions all over the world are readily available, which provide high resolution precipitation estimates with a wide spatial coverage including the African continent. SRS-based precipitation products are, however, subject to various error sources such as; cloud top reflectance, thermal radiance, sampling frequency, orbital drifts, topography, and precipitation retrieval algorithms (*Joyce et al.*, 2004; *Kummerow et al.*, 2004). Some SRS products utilize the high temporal resolution infrared (IR) measurements to estimate precipitation. The IR measurements are not directly related to precipitation, and hence, do not provide precise estimates at fine scales. The microwave measurements are more precise, compared to IR, but with lower temporal resolution (see, e.g., *Xie and Arkin*, 1997; *Joyce et al.*, 2004; *Dinku et al.*, 2008). In addition, challenges such as frequent satellite and sensor failures, and short life-spans may cause data inhomogeneity (e.g., *Kummerow et al.*, 2004), and consequently, long-term inconsistency. Due to the multiple limitations faced by the satellite-based products, data validation and uncertainty estimation of rainfall products are, therefore, necessary before using them in hydrological and climate studies, drought monitoring, and other related applications.

Various studies have been conducted over Africa, which assess the suitability of several SRS-based precipitation products through their comparisons with RG observations. However, most of these studies were often faced with lack of access to and/or inadequate RG records and have subsequently focused on specific sub-regions or basins within the African continent with available RG records. These studies range from West Africa (e.g., *Nicholson et al.*, 2003a), Nile Basin (e.g., *Dinku et al.*, 2011; *Habib et al.*, 2012; *Haile et al.*, 2012), East Africa (e.g., *Funk and Verdin*, 2003; *Dinku et al.*, 2007; *Romilly and Gebremichael*, 2011), Zambezi Basin (e.g, *Bowden and Semazzi*, 2007; *Dinku et al.*, 2008; *Liechti et al.*, 2012), Sahel region (e.g., *Dinku et al.*, 2010a) to a collection of basins (*Thiemig et al.*, 2012). Therefore, a continent-wide validation of various SRS-based precipitation products is necessary to assess their level of suitability to be used in various meteorological and hydrological applications.

Although RG observations are usually considered as the most accurate rainfall measurements over a point, both RG and SRS-based precipitation products are vulnerable to errors, i.e., systematic, random, and gross errors (see, e.g., *Janowiak et al.*, 1998; *Nicholson et al.*, 2003a; *Hughes*, 2006). Consequently, both techniques do not produce the ideal rainfall estimates to be considered as reference for validation purpose, which is particularly the case for interpolated and spatially averaged rainfall products. Therefore, in this paper, the "three-cornered-hat" (TCH) method (*Gray and Allan*, 1974) is applied, in its generalized form (*Galindo and Palacio*, 1999), to evaluate the relative performances of different rainfall products over the African continent. The generalized TCH method allows for a relative comparison of at least three datasets based on their respective uncertainties without the need of *a priori* knowledge of their uncertainties (e.g., *Koot et al.*, 2006). The performance of TCH (in estimating the uncertainty of rainfall products) is compared to that of classical gauge-based validation over the continent in order to account for possible artificial skills in the TCH validation method. Due to the inaccessibility of continent-wide RG based data, the full data product of the Global Precipitation Climatology Centre (GPCC) was used as a proxy for validating six SRS-based rainfall products. These products include: (i) African Rainfall Climatology Version 2 (ARCv2), (ii) Climate Prediction Center (CPC) Morphing Technique (CMORPH), (iii) Tropical Rainfall Measuring Mission (TRMM 3B43), (iv) Global Satellite Mapping of Precipitation moving vector with Kalman filter (GSMaP-MVK), (v) Tropical Applications of Meteorology using SATellite (TAMSAT), and (vi) Precipitation Estimation from Remotely Sensed Information using Artificial Neural Networks (PERSIANN).

It should be mentioned here that the distribution of RG stations used in GPCC over the continent is rather sparse, and as such, the evaluation of SRS products against GPCC over certain regions such as Congo, Angola, Somalia, and the Sahara should be interpreted with caution. Additionally, some of the investigated SRS products (i.e., TRMM, ARCv2, and PERSIANN) are merged with the RG observations that are also used in GPCC (e.g., *Huffman et al.*, 2010). Consequently, validating such products based on GPCC are likely to be tendentious. Nonetheless, such validations are applied in a number of studies worldwide (see, e.g., *Smith et al.*, 2006; *Kidd et al.*, 2012; *Conti et al.*, 2014), and over Africa (see, e.g., *Adeyewa and Nakamura*, 2003; *Cattani et al.*, 2014) with some reasonable results. It should be clarified that GPCC data are not used as the reference for the TCH method in this study but rather to provide independent evaluation upon which the TCH results are compared. The six SRS products

are further validated over GHA using in-situ RG observations obtained from an external data source; the IGAD (Inter-governmental Authority on Development, Africa) Climate Prediction and Application Center (ICPAC).

In order to extract and compare the dominant patterns of precipitation variability (derived from different datasets) and their spreading behavior over the continent, the statistical method of complex empirical orthogonal function (CEOF) (*Preisendorfer*, 1988) is applied. CEOF serves as an extension of the traditional principal component analysis or empirical orthogonal function (PCA/EOF) technique, which allows the extraction of non-stationary (space- and time-variable patterns) from precipitation observations (*Forootan*, 2014, pages 32-36). Thus, CEOF is used to identify the propagation patterns of precipitation changes, derived from the SRS-based products over Africa.

The remainder of the study is organized as follows. In Section 2, a brief background on the continental climatic regime with specific focus on precipitation variability across the African continent is presented. The description of various satellite products and a brief overview of their algorithms are provided in Section 3, followed by the methodology in Section 4. In Section 5, the results are presented. Finally, in Section 6, the main finding of this study is summarized and concluded.

2. Study area

The African continent lies astride the equator and almost entirely within the tropics. Its northern and southern regions exhibit temperate climate due to the mid-latitude westerly winds (*Wamukonya et al.*, 2006). Considered the second driest region in the world after Australia, Africa is divided into six wide climatic zones based on the amount, duration, and seasonal distribution of rainfall (e.g., *Nicholson*, 1986; *Wamukonya et al.*, 2006). These zones are referred to as the Hyper Arid, Arid, Semi-Arid, Dry Sub-humid, Moist Sub-humid, and Humid, in this contribution (cf., Figure 1a for details). Seasonal variations are primarily controlled by the movement of the Inter-Tropical Convergence Zone (ITCZ), which is also referred to as the tropical rain belt (*Nicholson*, 2013). The ITCZ shifts between the equator and the Sahara Desert during the austral summer (i.e., December, January and February) and boreal summer (June, July and August), resulting in a dipolar seasonal rainfall pattern across the continent. During the transitional periods of MAM (March, April and May) and SON (September, October

and November), most rainfall is observed within 10° of the equator, reducing polewards.

3. Data

In this section, a description of the rainfall products used in the study is given. These products include six SRS rainfall products, available as satellite only and merged fields (satellite + RG data). GPCC data and gauge observations over GHA from ICPAC were used to provide independent validation of the TCH method. The data used in this study are summarised in Table 1.

3.1. Global Precipitation Climatology Centre (GPCC)

The GPCC product consists of precipitation data from more than 67,000 gauge stations worldwide (*Becker et al.*, 2013), making it one of the most comprehensive gauge-based rainfall data available. GPCC, through the World Meteorological Organization (WMO), has been collating global gauge records since 1989. In addition, GPCC also incorporates archives from the Global Telecommunication Systems (GTS), daily surface synoptic observations (SYNOP) messages, and monthly climatological data (CLIMAT messages). It also utilizes published global datasets from the Food and Agriculture Organization (FAO) FAOCLIM 2.0, Climate Research Unit (CRU) of the University of East Anglia, Global Historical Network (GHCN), as well as several regional datasets. GPCC provides various precipitation products at different resolutions for a wide range of applications (see, e.g., *Becker et al.*, 2013; *Schneider et al.*, 2013).

Full Data Product (GPCC-FD) provided at monthly time scales with a spatial resolution of 0.5° were used in this study. This data is the most accurate version of the GPCC products, and is intended for validation studies (*Becker et al.*, 2013). Figure 1b shows the spatial distribution of gauges with at least 10 years of observations. In Africa, the gauge density varies substantially with sparse gauge network distributed in the northern regions (e.g., over Chad, Niger, Libya, and Egypt), as well as central parts (e.g., Congo and Somalia) of the continent. The highest gauge density is found over Southern Africa, West Africa, and within the Lake Victoria basin, where each 0.5° grid contains more than 2 gauge stations. Additionally, Figure 1c shows temporal variations of number of stations between 2003–2010. The decline in the estimated station in 2009 is attributed to the fact that most of the WMO member countries contributed data only

up 2008 with the remaining 2 years (2009-2010) based on GTS records and data from some donor countries (*Becker et al.*, 2013, see references therein).

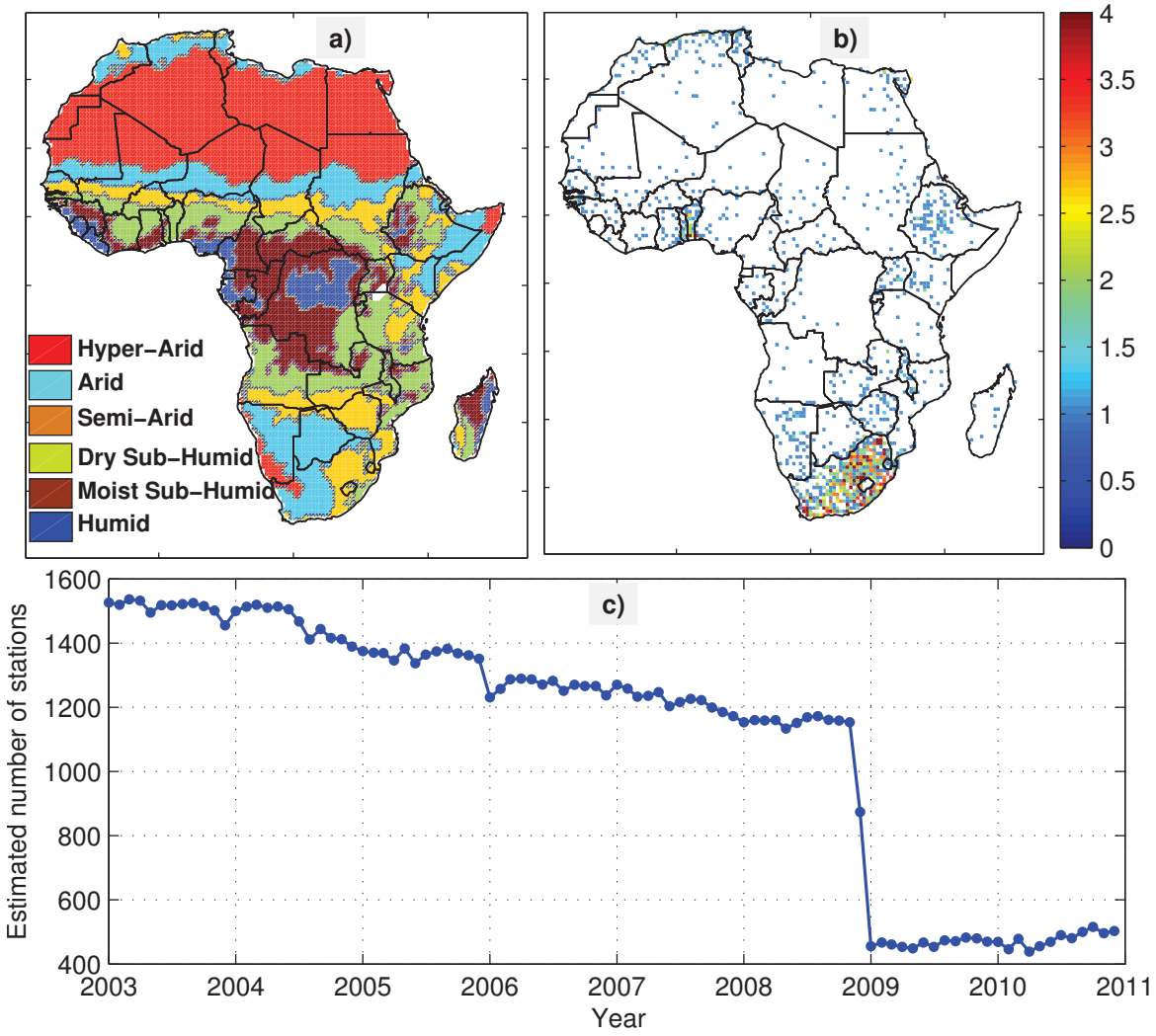

Figure 1: (a) Climate zones in Africa based on seasonal rainfall amount and duration, (b) approximate number of rain gauge stations per 0.5°×0.5° grid in the GPCC-FD product averaged for the period 2003 to 2010, and (c) number of the gauge stations per month for the period 2003 to 2010.

3.2. African Rainfall Climatology Version 2 (ARCv2)

ARCv2 is a revised version of Climate Prediction Center's (CPC) African Rainfall Climatology (ARC), which provides African precipitation from 1983. It provides daily precipitation fields based on a subset of source data from Rainfall Estimate version 2 (RFE2) algorithm at a spatial resolution of 0.1° (*Novella and Thiaw*, 2013). ARCv2 input dataset consists of

data from a 3-hourly geostationary infrared (IR) sensor centered over Africa by the European Organization for the Exploitation of Meteorological Satellites (EUMETSAT) and the Global Telecommunication System (GTS) gauge observations. The main difference between RFE2 and ARCv2 is that, the latter does not contain passive microwave (MW) data in its algorithm.

3.3. Climate Prediction Center (CPC) Morphing Technique (CMORPH)

CMORPH is a high resolution global precipitation analysis technique, developed at the National Oceanic and Atmospheric Administration (NOAA)'s Climate Prediction Center (CPC) for rainfall estimation (see, e.g., *Joyce et al.*, 2004). It produces precipitation estimates between 60°N and 60°S with a spatial resolution of 0.073° (at the equator) and a temporal resolution of the 30 minutes. Daily fields are produced by accumulating 30-minute segments over a 24-hour period. The precipitation estimates from the low earth orbiting (LEO) satellite microwave scans are propagated by motion vectors derived from geostationary satellite's IR data. This technique utilizes the advantages of two satellite rainfall estimates, where a more direct measurement but a relatively poor resolution passive microwave observations are integrated with low quality but high resolution IR precipitation estimates. The CMORPH precipitation estimates have been extended back from December 2002 to the TRMM-era (1998-present) and reprocessed from 2003 using the most recent version of PMW algorithm and IR observations (*Xie et al.*, 2015). For this study, we used the earlier version of CMORPH from 2003 to 2010. This dataset is not merged with *in-situ* RG observations.

3.4. Global Satellite Mapping of Precipitation moving vector with Kalman filter (GSMaP-MVK)

The GSMaP-MVK (hereafter referred to as GSMaP), a product of the Japan Aerospace Exploration Agency (JAXA), is a multi-satellite precipitation data source. A Kalman filtering technique is used to estimate hourly global precipitation at a spatial resolution of 0.1°. GSMaP merges data from passive microwave sources (i.e., TRMM Microwave Imager - TMI, Advanced Microwave Scanning Radiometer for EOS - AMSR-E, Special Sensor Microwave/Imager - SSM/I) and infrared (IR) images to compute moving vector fields. Based on the moving vector fields calculated from successive IR images, precipitation fields are propagated and refined in a Kalman filtering process (see, e.g., *Ushio and Kachi*, 2010). This product is not merged with RG observations. The hourly products from 2003 to 2010 were converted to monthly precipitation fields in this study.

3.5. Precipitation Estimation from Remotely Sensed Information using Artificial Neural Networks (PERSIANN)

PERSIANN is a product of the Center for Hydrometeorology and Remote Sensing (CHRS) of the University of California, and is available from March 2000 at a spatial resolution of 0.25°, and at 3-hourly and 6-hourly temporal scales. The PERSIANN algorithm employs a neural network to optimally combine infrared images of the geostationary environmental satellite, the TRMM Microwaver Imager (i.e., the TMI 2A12 product), and is calibrated with the Global Precipitation Climatology Project product (GPCP) (*Sorooshian et al.*, 2000; *Hsu and Sorooshian*, 2008). For this study, 6-hourly products of 2003 to 2010 were converted to monthly rainfall estimates.

3.6. Tropical Applications of Meteorology using Satellite data and ground-based observations (TAMSAT)

TAMSAT is an Africa-specific precipitation data source available at 0.0375° spatial resolution. The dataset is available since 1983 at decadal, seasonal, and monthly time scales. Its algorithm is based on assumptions that a large portion of precipitation over Africa is usually derived as a result of convective clouds, and secondly, the existence of a linear relationship between cold cloud duration (CCD) and precipitation events (e.g., *Grimes et al.*, 1999). As such, it is well suited for regions characterized mostly by convective rainfall. The algorithm estimated rainfall is not merged with contemporaneous RG data but calibrated with historical data that is considered time invariant (see, e.g., *Maidment et al.*, 2013).

3.7. Tropical Rainfall Measuring Mission (TRMM)

Gridded rainfall estimates from TRMM Multisatellite Precipitation Analysis (TMPA, *Huffman et al.*, 2007) are available from the National Aeronautics and Space Administration (NASA) Goddard Space Flight Center (GSFC) since 1998. TMPA precipitation products are an integrated rainfall estimates from various sensors such as Precipitation Radar (PR), Special Sensor Microwave Imager (SSM/I)), and infrared (IR) a board a geostationary satellites. Additionally, the products are merged with RG observations from the GPCC. The data is available at a spatial resolution of $0.25° \times 0.25°$ with a spatial coverage between 50°S to 50°N, at a 3-hourly and monthly time scales. Validation of TRMM and its merged precipitation products are crucial due to the aging of the satellites, which was initially planned for a 5 year life span (see, e.g.,

Kummerow et al., 1998), but have now been in orbit for over a decade. For this study, monthly precipitation products of TRMM-3B43 version 7 from TMPA are used and are referred to as TRMM, hereafter.

3.8. Rain gauge data over Greater Horn of Africa (GHA)

Daily *in-situ* observations from 54 rain gauge stations, spread almost over the entire GHA, were obtained from IGAD (Inter-governmental Authority on Development, Africa) Climate Prediction and Application Center (ICPAC). The *in-situ* data covers the duration (1961-2009) but with gaps in most individual RG station records, see also *Omondi et al.* (2014). Of the available 54 RG stations, only 30 stations (mainly located in Kenya, Ethiopia, and Tanzania) for the period of 2003 to 2007 had consistent records, and were subsequently used in the analysis.

Table 1: Summary of the data used in this study.

Product	Temporal Availability	Spatial Resolution [lat x lon]	Temporal Resolution	Coverage	Data used
In-Situ data	–	54 stations	Daily	GHA	2003-2007
GPCC	1900-2010	0.5° x 0.5°	Monthly	Global-land only	0.5° x 0.5° at monthly scale between 2003-2010
ARCv2	1983-present	0.10° x 0.10°	3-hourly	Africa	
CMORPH	1998-present	0.25° x 0.25°	3-hourly	50°S × 50°N	
GSMaP_MVK	2002-2010	0.10° x 0.10°	1-hourly	60°S × 60°N	
PERSIANN	2000-2014	0.25° x 0.25°	6-hourly	50°S × 50°N	
TAMSAT	1983-present	0.0375° x 0.0375°	Monthly	Africa	
TRMM 3B43v7	1998-present	0.25° x 0.25°	Monthly	50°S × 50°N	

4. Methodology

All the high resolution SRS-based products (Table 1; ARCv2, CMORPH, GSMaP, PERSIANN, TAMSAT, and TRMM) were bi-linearly interpolated to the standard grid resolution of GPCC data (i.e., $0.5° \times 0.5°$), while 3-hourly or 6-hourly products were summed to monthly product. Similarly, daily gauge observations from the GHA region (i.e., Table 1) were converted to monthly rainfall accumulations (mm/month). To account for the spatial mismatch between RG observations and gridded precipitation estimates over the GHA region, monthly *in-situ* observations and corresponding values from gridded products were spatially-averaged according

to the existing climatic regimes as discussed in, e.g., *Bowden and Semazzi* (2007) and *Omondi et al.* (2014).

Various approaches were employed to assess the gridded precipitation estimates, including comparison with the gauge-based GPCC product. Inter-comparisons of uncertainties in precipitation estimates from individual gridded products were performed using the generalized TCH method, and complex empirical orthogonal function (CEOF) employed to assess the spatio-temporal behavior of these precipitation products over the African continent. These methods are briefly described below.

4.1. Generalized three-cornered hat method

While GPCC is considered as a reliable source of gauge-based precipitation data on the continental scale, there still exists large data gaps over various regions of Africa (cf. Figure 1b), mostly caused by lack of data sharing from these regions (*Nicholson et al.*, 2003a). Thus, using GPCC product as the reference data to assess the satellite-derived rainfall estimation over these regions may be less reliable or even introduce additional bias to the gauge-adjusted products. Additional circumstances include the lack of consistency in the number of reporting gauges over time (see, Figure 1c) and challenges in timely updating the gauge records in GPCC. The three-cornered hat (TCH) on the other hand, can be used to estimate relative uncertainties in rainfall products from different sources if at least three products are available (e.g., *Tavella and Premoli*, 1994). The generalized TCH method is particularly relevant in this study as it accounts for the dependency between different precipitation estimates. In this particular contribution, the TCH method is extended to include the six SRS-based precipitation products presented in Table 1. The same approach has been used by *Koot et al.* (2006) to assess the quality of each individual time series of atmospheric angular momentum from five different meteorological centers.

To estimate the uncertainty in precipitation datasets, consider the time series of available products stored as $\{\mathbf{x}_i\}_{i=1,2,\cdots,N}$, where i corresponds to each product (i.e., $N = 6$, six SRS-based rainfall products in Table 1). Let each time series be expressed as

$$\mathbf{x}_i = \mathbf{s} + \varepsilon_i, \quad \forall i = 1, \ldots, N, \tag{1}$$

where $\mathbf{s}$ is the true signal and ε_i is a zero-mean white noise process representing the measurement error of the SRS-based rainfall i. Since no true estimate of $\mathbf{s}$ is available, the differences between each time series and one of them arbitrarily chosen as the reference is computed as (*Koot et al.*, 2006):

$$\mathbf{y}_i \equiv \mathbf{x}_i - \mathbf{x}_R = \varepsilon_i - \varepsilon_R, \quad i = 1, \ldots, N-1, \tag{2}$$

with $\mathbf{x}_R$ being the arbitrarily chosen reference time series. For this study TRMM time series was chosen as the reference time series. It is important to note that the results of the uncertainty estimations are independent of choice of reference time series since the computations are based on the covariance of the differences in Equation 2. In Example 1, it is demonstrated that the choice of the reference does not influence the final results of the TCH method. Therefore, selecting any of the remotely sensed precipitation products, other than TRMM time series, as reference, will not alter the findings (see, e.g., *Tavella and Premoli*, 1994; *Koot et al.*, 2006). Indeed, GPCC was tested as reference (results not shown) and provided similar results to those reported in this study.

The samples of the $N-1$ SRS-based precipitation differences (Equation 2) are stored in the columns of a $M \times (N-1)$ matrix as:

$$\mathbf{Y} = \begin{bmatrix} \mathbf{y}_1 & \mathbf{y}_2 & \cdots & \mathbf{y}_{(N-1)} \end{bmatrix}, \tag{3}$$

where each row is a monthly observation (here $M = 96$, i.e., 96 months from 2003-2010). The covariance matrix $\mathbf{S}$ of the series of differences given by

$$\mathbf{S} = \mathrm{cov}(\mathbf{Y}), \tag{4}$$

where $\mathrm{cov}(\circ)$ is the covariance operator, and elements of $\mathbf{S}$ ($s_{i,j}$) being either variance estimates (for $i = j$) or covariance estimates (for $i \neq j$) otherwise. Introducing the unknown $N \times N$ covariance matrix of the individual noises $\mathbf{R}$, it is related to $\mathbf{S}$ by (*Galindo and Palacio*, 2003)

$$\mathbf{S} = \mathbf{J} \cdot \mathbf{R} \cdot \mathbf{J}^T, \tag{5}$$

where the matrix $\mathbf{J}$ is given by

$$\mathbf{J}_{(N-1)N} = \begin{bmatrix} 1 & 0 & \cdots & 0 & -1 \\ 0 & 1 & \cdots & 0 & -1 \\ \vdots & \vdots & \ddots & \vdots & \vdots \\ 0 & 0 & 0 & 1 & -1 \end{bmatrix}. \tag{6}$$

Equation 5 is undetermined because there are $N \times (N+1)/2$ unknowns (number of distinct elements of $\mathbf{R}$), but only $N \times (N-1)/2$ equations (number of distinct elements of $\mathbf{S}$). Thus, there remain N "free" parameters that must be reasonably determined to obtain a unique solution (*Galindo and Palacio*, 2003).

An important constraint on the solution domain for the free parameters, however, is that the estimated covariance matrix $\mathbf{R}$ must be positive definite (Koot et al., 2006), i.e., $|\mathbf{R}| > 0$ (*Galindo and Palacio*, 2003). This condition restricts the solution domain for the free parameters ($r_{iN}, \ldots, r_{NN}$, $i = 1, \ldots, N-1$), but nevertheless, it is not sufficient to determine them (Koot et al., 2006). The free parameters are thus chosen in such a way that the sum of the estimated correlations between all the time series is minimal considering the constraint $|\mathbf{R}| > 0$. To determine the N free parameters, a suitable objective function should be defined. The suggested objective function is given by (*Galindo and Palacio*, 1999) as

$$F(r_{1N}, \cdots, r_{NN}) = \sum_{i<j}^{N} \frac{r_{ij}^2}{K^2}, \tag{7}$$

where $K = \sqrt[N-1]{|\mathbf{S}|}$. The solution of the minimization problem is found based on the Kuhn-Tucker theorem (*Galindo and Palacio*, 1999). Hence, when the free parameters have been estimated, the solution for the other unknown elements of $\mathbf{R}$ is given by

$$r_{ij} = s_{ij} - r_{NN} + r_{iN} + r_{jN}, \quad i, j = 1, \cdots, N-1, \tag{8}$$

and s_{ij} obtained from Equation 4.

Example 1 (Choice of the TCH reference): Consider the following numerical example where we have 3 time series A, B, and C as shown in Figure 2 whose quality is to be determined. Now from Table 2, let the time series "C" in the first column, "B" in the second column, and "A" in the third column be chosen as a reference. Considering "C" as the reference, the diagonal of

R shows the variances of A, B, and C as diagonal elements, respectively. With "B" as reference, the variances of A, C, and B are given respectively as diagonal elements. Finally, with "C" as reference, the variances of B, C, and A are given in the diagonal elements in the third column, respectively. As can be seen from the results, the choice of the reference is immaterial as the same results are obtained irrespective of the chosen reference.

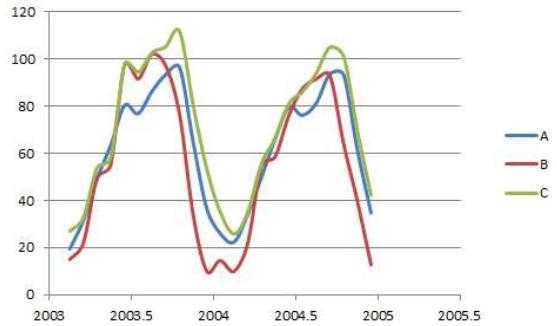

Figure 2: A sample time series of 3 datasets A, B, and C used to demonstrate the TCH method.

Table 2: Example of TCH algorithm.

C ("reference")	**B ("reference")**	**A ("reference")**
$S = cov(A-C, B-C)$	$S = cov(A-B, C-B)$	$S = cov(B-A, C-A)$
$S = \begin{bmatrix} 40.51 & 23.46 \\ 23.46 & 220.12 \end{bmatrix}$	$S = \begin{bmatrix} 213.72 & 196.67 \\ 196.67 & 220.12 \end{bmatrix}$	$S = \begin{bmatrix} 213.72 & 17.05 \\ 17.05 & 40.51 \end{bmatrix}$
$R = \begin{bmatrix} 17.05 & 0 & 0 \\ 0 & 196.67 & 0 \\ 0 & 0 & 23.46 \end{bmatrix}$	$R = \begin{bmatrix} 17.05 & 0 & 0 \\ 0 & 23.46 & 0 \\ 0 & 0 & 196.67 \end{bmatrix}$	$R = \begin{bmatrix} 196.67 & 0 & 0 \\ 0 & 23.46 & 0 \\ 0 & 0 & 17.05 \end{bmatrix}$

4.2. Performance ranking of the SRS-based precipitation products

Estimating the magnitude of noise is not adequate to describe the relative quality of each rainfall product. Thus, for each SRS product, the signal-to-noise ratio (SNR) is estimated considering the time series of precipitation for grid points as (e.g., *Seo et al.*, 2006)

$$\mathrm{SNR} = \frac{\mathrm{RMS}(t)}{\sigma}, \quad \text{or in case of the RMSE as } \mathrm{SNR} = \frac{\mathrm{RMS}(t)}{\mathrm{RMSE}}, \tag{9}$$

where RMS is the root-mean-square of the SRS-based products for the time (t) period 2003 to 2010 at each grid point, and σ indicates the magnitude of uncertainties from the TCH method. In ranking the products, a higher SNR is considered better than a lower SNR.

4.3. Multiple comparison procedure (MCP)

In order to rank, as well as to determine the similarities (or dissimilarities) of the available precipitations products over Africa, a multiple comparison procedure (MCP) (see, e.g., *Day and Quinn*, 1989) based on the information in the root-mean-squares-errors (RMSE), uncertainties, and their respective SNR values was carried out by first performing the non-parametric Kruskal-Wallis test (*McKight and Najab*, 2010) at 95% confidence interval, followed by the Tukey-Kramer test (*Rafter et al.*, 2002). The Krustal-Wallis test ranks each of the products based on their performance measures, while the Tukey-Kramer test measures the similarities and dissimilarities among the precipitation products.

4.4. Complex empirical orthogonal function (CEOF)

Given the wide variety of blended precipitation products and different precipitation retrieval methods (Table 1), it is important that all the gridded precipitation estimates provide consistent spatial and temporal patterns over various regions of Africa. This is examined by applying CEOF (*Preisendorfer*, 1988) to the time series derived from each of the gridded precipitation products (7 products of Sections 3.1 to 3.7, i.e., Table 1, individually), and extracting their main spatio-temporal behavior. To perform CEOF, the Hilbert Transform of the original rainfall time series was added as their imaginary part to produce new sets of complex time series. The Hilbert transform introduces a phase shift of $\frac{\pi}{2}$ (in the frequency domain) to the original rainfall time series. The generated complex data sets therefore contain information on the changes in rainfall and their temporal-rates of change (see e.g., *Forootan*, 2014, pages 32-36 for details). Singular value decomposition (SVD, *Preisendorfer*, 1988) method is applied to decompose the generated complex data sets resulting in complex spatial patterns, known as the complex empirical orthogonal functions (CEOFs), and the temporal patterns of complex principal components (CPCs). Both CEOFs and CPCs contain real and imaginary parts, which are used to derive the dominant modes of rainfall variability in terms of amplitudes and phases that are usually better suited in extracting spreading patterns such as rainfall fluxes (see e.g., *Cromwell*, 2006).

5. Results

The quality of the available rainfall products is evaluated using three different methods over the common period of 2003-2010. First, the SRS-based rainfall products are evaluated with respect to the GPCC dataset over the whole African continent using standard statistical measures such as relative bias, RMSE, and correlation coefficients. Secondly, the generalized "three-cornered-hat" (TCH) method is applied to assess the uncertainties of all the gridded precipitation products. The evaluations are carried out on a continent-wide, as well as over the six prominent climatological regimes of Africa shown in Figure 1a. Monthly precipitation products are then ranked based on the evaluation results using multiple comparison procedure (MCP). Additionally, a special case of GHA is considered, where *in-situ* RG observations are used to assess the results of TCH and the classical rain gauge (RG)-based validations (i.e., from GPCC). Thirdly, CEOF is employed to assess the spatio-temporal patterns of rainfall variability over Africa. It should be mentioned that the choice of the precipitation products depends also on the application, and the recommendations based on the performed analyses, may not necessarily benefit all applications, particularly since the evaluations are carried out at monthly scales.

5.1. GPCC-based evaluation of SRS-based precipitation estimates (2003-2010)

Figure 3 shows the spatial distribution of monthly mean biases, RMSE, and correlation coefficients of various SRS-based rainfall estimates with respect to GPCC over Africa for the period 2003 to 2010. From Figure 3, it can be seen that gauge-adjusted satellite products (TRMM, ARCv2, and PERSIANN) are more consistent with GPCC than the satellite-only products (CMORPH and GSMaP). TRMM precipitation estimates are adjusted using the latest GPCC re-analysis data, and therefore, indicate the closest agreement in all three metrics (bias (Figure 3f), RMSE (Figure 3i), and correlation (Figure 3r)). It is closely followed by the IR-reliant PERSIANN product and the African-specific ARCv2 data with relatively low RMSEs and higher correlation coefficients over most of Africa. However, PERSIANN tends to deviate more (in relation to GPCC) compared to ARCv2 product. Additionally, in relation to GPCC, TAMSAT consistently underestimates rainfall over most areas of Africa and also indicates lower correlation with GPCC over the Sahara region. In general, among the gauge-adjusted satellite rainfall estimates, ARCv2 and PERSIANN tend to show less correlations with GPCC over data-

sparse regions of Sahara and Congo, as well as Somalia than those rainfall anomalies derived from TRMM (Figure 3 (m), (p), and (r)). Due to the sparse distribution of GPCC products over these regions (see Figure 1), however, the derived evaluations have to be interpreted with caution.

Satellite-only products CMORPH and GSMaP, on the other hand, indicate very large positive differences (up to 100 mm/month) over the high rainfall regions of central Africa (e.g., Congo), and the African rain belt region. Large negative differences are also found over the orographic regions of Ethiopia, Kenya, and Tanzania. Substantial underestimations in relation to GPCC are also prevalent over the coastal regions of eastern Madagascar and southern Liberia, which are also seen in ARCv2, PERSIANN, and TAMSAT products. Very low correlation coefficients are also found in the arid regions and along the coastal regions (see Figure 3).

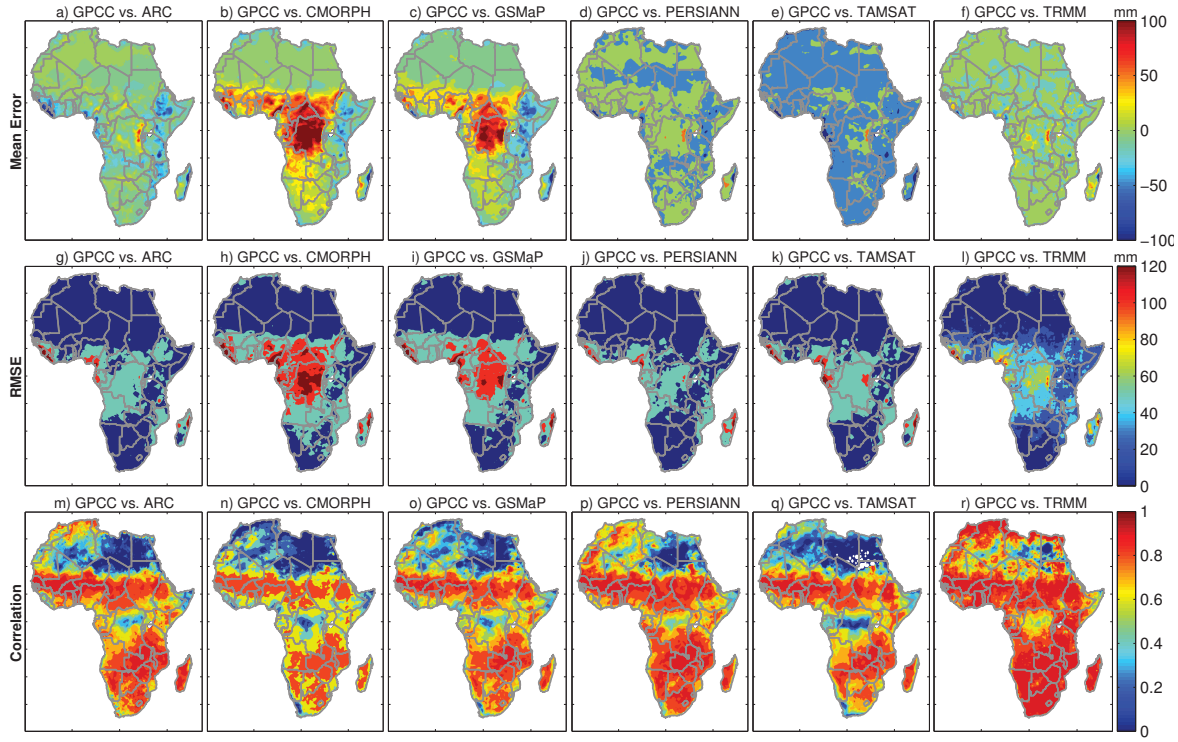

Figure 3: Mean biases (a-f), RMSEs (g-l), and correlation coefficients (m-r) of six SRS-based precipitation estimates relative to the GPCC gauge-based rainfall products over Africa for the period 2003 to 2010.

The microwave dominant estimates of rainfall (e.g., CMORPH) are also prone to underestimate the rainfall amount over local convective zones and orographic regions like those over the Ethiopian Highlands and east coast regions of Madagascar. This underestimation is related to the local convection during the orographic lifting of the south-westerlies, which are generally

characterized by shallow clouds with very low ice content (*Nesbitt et al.*, 2008; *Habib et al.*, 2012). This process leads to significant underestimation in microwave-based estimates because of their direct relationship with ice-hydrometeors. Equivalent underestimations were also found in the IR-dominant products such as ARCv2 over these orographic and local convection regions. *Dinku et al.* (2007) compared RFE versions 1 and 2 (RFE2 is the precursor of ARCv2) and reported that RFE1 performed better than RFE2 as it takes into account, the orographic warm rain process. On the other hand, the IR-based precipitation estimates (e.g., ARCv2 and PERSIANN) tend to show relatively lower magnitudes of bias and RMSE in the convective regions (e.g, Congo region) as opposed to the microwave-based estimates. It is worth mentioning that these products incorporate gauge datasets from GTS reporting stations, and subsequently show relatively lower RMSE than TRMM over the Congo region.

Table 3 provides the performance rankings of the individual SRS-based precipitation products in decreasing order of SNR magnitudes. The SNR values are derived as ratios of individual RMS values to RMSE estimates relative to the gauge-based GPCC products (e.g.,Equation 9. It can be seen that precipitation estimations from TRMM represent the closest resemblance to those of GPCC over all the climatic regimes, as well as over the whole continent due to their inter-dependency (i.e., TRMM incorporating GPCC data). The estimations derived from PERSIANN also indicate equally good performance for all the regions, while the region-specific product ARCv2 tend to perform better over the arid regions. The results of other SRS-based products (TAMSAT, CMORPH, and GSMaP) tend to vary over various climatic regions, although CMORPH seem to be better suited over the arid regions. Therefore, in terms of the correctly characterizing spatial and temporal amplitude variations over Africa with respect to GPCC for the 2003-2010 study period, the products are ranked in the order: TRMM, PERSIANN, ARCv2, TAMSAT, CMORPH, and GSMaP.

5.2. Uncertainty analysis using the generalized Three-Cornered-Hat (TCH) method

As discussed in Section 4.1, the generalized TCH method offers a simple and efficient way of quantifying relative error estimates in different datasets of the same variable. While to apply the method one still requires to choose a set of observation as a reference data, such choice does not affect the overall estimate of error as illustrated in Example 1. In this study the uncertainty estimates in Figure 4(a-f) are derived by applying TCH method considering TRMM products as the reference. It can be seen from Figure 4 that the magnitude of uncertainties are generally

Table 3: Performance of various SRS-based rainfall estimates ranked according to the decreasing magnitude of SNRs over different climatic regimes (see, Figure 1), as well as for the whole continent. The shaded products indicate statistically similar order of magnitudes.

REGION\RANK	1	2	3	4	5	6
	A) MCP ranks based on RMSE					
CONTINENT-WIDE	TRMM	PERSIANN	ARCv2	TAMSAT	CMORPH	GSMaP
HUMID	TRMM	PERSIANN	ARCv2	TAMSAT	CMORPH	GSMaP
MOIST SUB-HUMID	TRMM	PERSIANN	ARCv2	TAMSAT	CMORPH	GSMaP
DRY SUB-HUMID	TRMM	PERSIANN	ARCv2	TAMSAT	CMORPH	GSMaP
SEMI ARID	TRMM	ARCv2	PERSIANN	TAMSAT	CMORPH	GSMaP
ARID	TRMM	ARCv2	PERSIANN	TAMSAT	CMORPH	GSMaP
HYPER ARID	TRMM	PERSIANN	TAMSAT	ARCv2	CMORPH	GSMaP
	B) MCP ranks based on SNR					
CONTINENT-WIDE	TRMM	PERSIANN	ARCv2	CMORPH	TAMSAT	GSMaP
HUMID	TRMM	PERSIANN	CMORPH	ARCv2	GSMaP	TAMSAT
MOIST SUB-HUMID	TRMM	PERSIANN	CMORPH	ARCv2	TAMSAT	GSMaP
DRY SUB-HUMID	TRMM	PERSIANN	ARCv2	CMORPH	TAMSAT	GSMaP
SEMI ARID	TRMM	PERSIANN	ARCv2	CMORPH	TAMSAT	GSMaP
ARID	TRMM	PERSIANN	ARCv2	CMORPH	TAMSAT	GSMaP
HYPER ARID	TRMM	PERSIANN	CMORPH	ARCv2	GSMaP	TAMSAT

higher in the high rainfall regions, while over the arid and semi-arid regions, considerably lower magnitudes of uncertainties are found (see the patterns of Figure 4(g-l) and the discussion in Section 5.3). Based on these results, the magnitude of uncertainties in PERSIANN and ARCv2 are found to be lower than those of CMORPH and GSMaP. This is in agreement with the general assessment carried out in Section 5.1 (see, e.g., Figure 3), where satellite-only products showed large positive biases and RMSEs over these region.

The distributions of noise estimates over the entire continent are presented in Figure 5a, while the results of the MCP ranking are provided in Table 4. From Figure 5a, the uncertainties in the PERSIANN estimates represent the smallest median followed by ARCv2, TRMM, and TAMSAT products in an ascending order of magnitude. CMORPH and GSMaP products indicate high median magnitudes of noise estimates, as well as relatively large inter-quartile range (IQR), while ARCv2 and TAMSAT are statistically similar over the continent. It is apparent that noise in the merged products (PERSIANN, ARCv2, TAMSAT, and TRMM) are lower than those of the un-merged products (CMORPH and GSMaP). This demonstrates

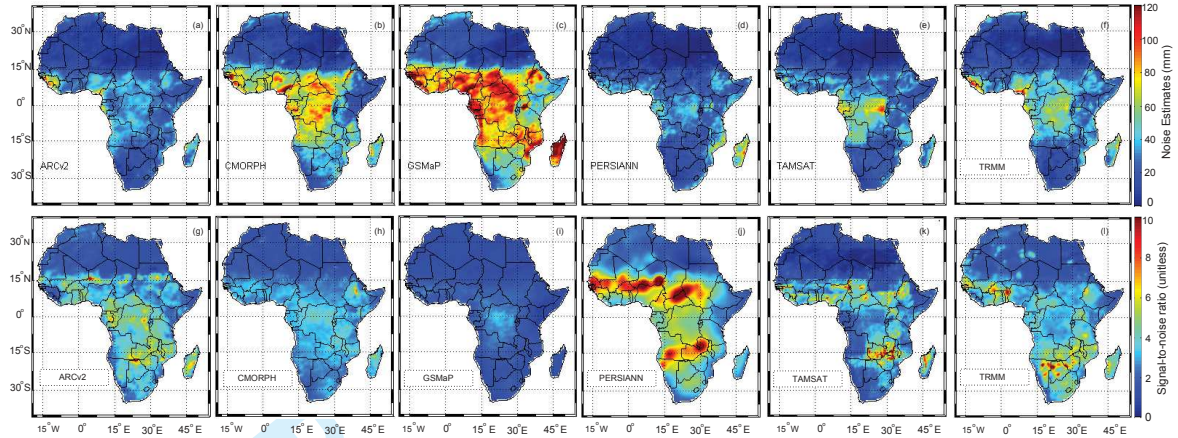

Figure 4: (a-f) Uncertainties of various SRS-based precipitation products over Africa based on the TCH method, and (g-l) their corresponding SNR values based on Equation 9. GPCC is not included as only SRS-based data are evaluated

the effectiveness of adjusting satellite products with gauge observations, in agreement with *Nicholson et al.* (2003b).

The uncertainties in the precipitation products are generally reduced from the wet regions to the dry areas as seen from the summaries of the relative performances of the different products Figure 5(b-g, see the height of box plots). PERSIANN performed better than the other rainfall products in all climatic zones followed by ARCv2. A summary of MCP rankings corresponding to different products in the climatic zones of Figure 1, as well as the entire continent is provided in Table 4 (compare with Table 3 for GPCC). The noise estimates from PERSIANN indicate the highest rank (lowest noise magnitudes) over all sub-climatic zones. In all but the semi-arid and hyper-arid regions, the rank of the other products are ordered as: ARCv2, TAMSAT, TRMM, CMORPH and GSMaP, where GSMaP is ranked the least (with the highest uncertainties). In the semi-arid region, noise estimates in TAMSAT are smaller than ARCv2, however, the two products along with TRMM are found to be statistically similar. Additionally, TAMSAT and TRMM represent better quality than ARCv2 in the hyper-arid zone. The results show that PERSIANN and ARCv2 are not significantly different in the humid zone, whereas ARCv2 and TAMSAT are similar in the dry-sub humid zone.

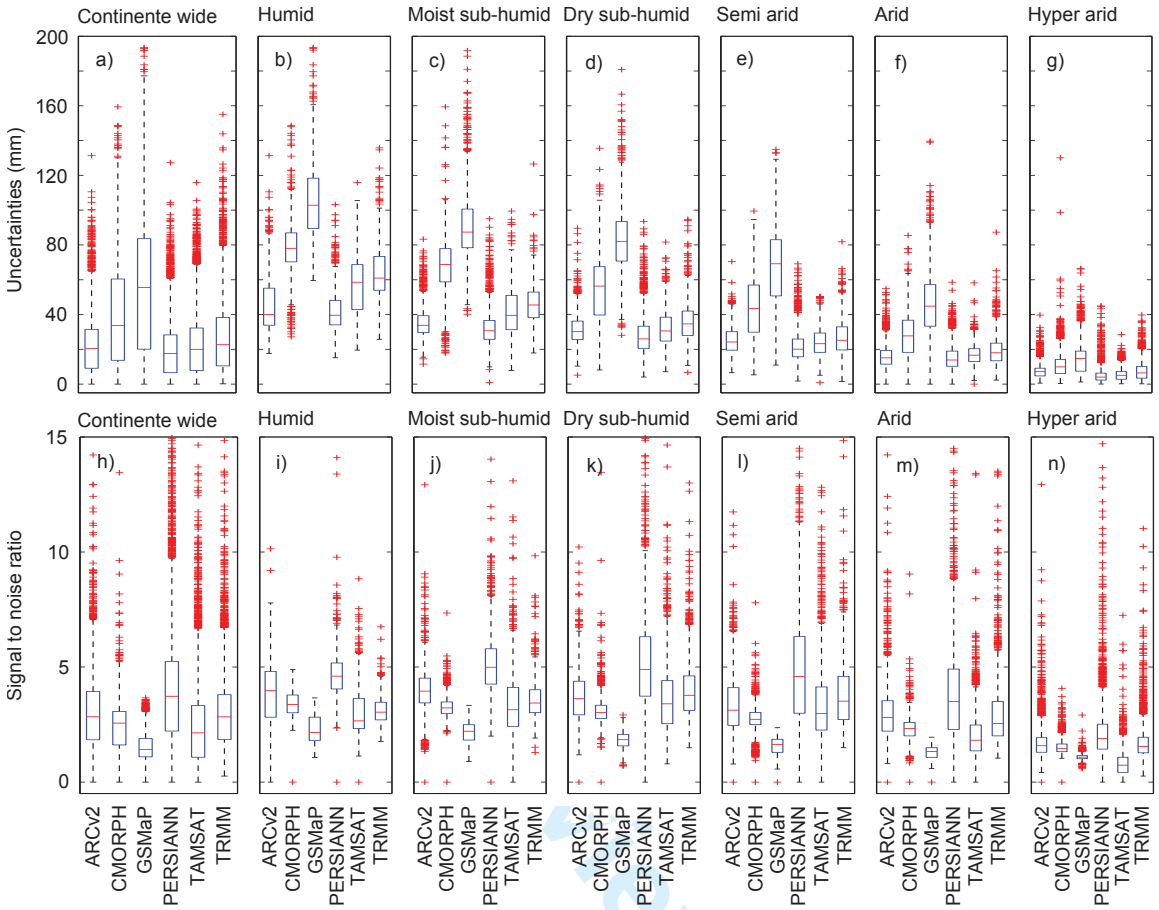

Figure 5: Box plot summaries of (a-g) average relative noise estimates over Africa, as well as for the six climatic regimes as shown in Figure 1, and (h-n) represent the corresponding SNR values. The whiskers indicate maximum and minimum range of the noise estimates while the box shows the interquartile (first and third quartile) range of variation. The segment inside the box shows the median of the data and the red marks above or below the whiskers indicate the outliers.

5.3. Signal-to-noise ratios (SNRs)

5.3.1. Continent-wide SNRs

As stated in Section 4.2, the noise measurements are by themselves not enough to rank the overall performances of different rainfall products as those that represent lower amplitudes of rainfall variations usually contain lower noise values. Consequently, the SNR for each product was estimated in order to assess their relative performances as a ratio of their respective RMS to noise estimates, see Figure 4(g to l). The spatial patterns of SNRs are similar to that of the noise distributions, indicating lower values in the drier areas and higher values in wetter regions. The spatial average of the noise estimates over the entire Africa is shown in Figure

5a. The relative performances over the continent through the MCP rankings are presented in Table 4, which indicates that PERSIANN has the highest performance followed by ARCv2, TRMM, CMORPH, TAMSAT, and GSMaP in that order. Statistically, ARCv2 and TRMM are found to be similar over the continent.

5.3.2. SNRs within climate zones

The spatial average of SNRs over the entire continent is presented in Fig 5(h), while the performances of the products in all the six rainfall regions (cf., Figure 1a), in terms of SNRs, are shown in Figure 5(i to n) and Table 4. From the values in Table 4, one can conclude that PERSIANN represents the highest SNR in all regions, while GSMaP is ranked the least in all but the hyper-arid areas, where TAMSAT showed the smallest SNR. In the humid region, ARCv2 was ranked after PERSIANN, while CMORPH outperformed TRMM. In the moist sub-humid, the performances of the assessed products after PERSIANN are as follows: ARCv2, TRMM, TAMSAT, CMORPH, and GSMaP. TAMSAT and CMORPH are found to be statistically similar. In the dry sub-humid and semi-arid zones, the products ranks are ordered as: TRMM, ARCv2, TAMSAT, CMORPH, and GSMaP, while the rank in the arid region is found as: ARCv2, TRMM, CMORPH, TAMSAT and GSMaP. The order in the hyper-arid zone is similar to that of the arid zone, however, GSMaP indicated better results than TAMSAT. It is worth noting that SNRs in the arid and hyper-arid regions are found to be lower than those in other regions, see Figure 5(m and n). This is consistent with the findings in *Dinku et al.* (2010a), who suggested that sub-cloud evaporation, rainfall suppression by desert aerosols, and surface effects among other error sources severely affect satellite rainfall estimation in drier parts of the continent.

5.4. Quality of the rainfall products over the Great Horn of Africa

The point-based *in-situ* observations and the corresponding grids values of rainfall from available products are spatially averaged according to the three climatological regimes (e.g., *Omondi et al.*, 2014): a) the northern sector (Ethiopia and Eritrea with 8 stations), b) equatorial sector (Kenya and Rwanda with 16 stations), and c) the southern sector (Tanzania with 6 stations mainly over the coastal areas) in order to provide a fair comparison. Figure 6(a-c) shows the mean seasonal cycle of rainfall over the three regions. The three climatological regimes in GHA represent completely different rainfall regimes with the northern sector showing

Table 4: Performance of the six SRS-based rainfall estimates over Africa ranked according to the decreasing magnitude of SNRs derived from the TCH method. The shaded products indicate statistically similar order of magnitudes.

REGION \RANK	1	2	3	4	5	6
A) MCP ranks based on uncertainty levels						
CON	PERSIANN	ARCv2	TAMSAT	TRMM	CMORPH	GSMaP
HU	PERSIANN	ARCv2	TAMSAT	TRMM	CMORPH	GSMaP
MSH	PERSIANN	ARCv2	TAMSAT	TRMM	CMORPH	GSMaP
DSH	PERSIANN	ARCv2	TAMSAT	TRMM	CMORPH	GSMaP
SA	PERSIANN	TAMSAT	ARCv2	TRMM	CMORPH	GSMaP
Ar	PERSIANN	ARCv2	TAMSAT	TRMM	CMORPH	GSMaP
HA	PERSIANN	TAMSAT	TRMM	ARCv2	CMORPH	GSMaP
B) MCP ranks based on SNRs						
CONTINENT-WIDE	PERSIANN	ARCv2	TRMM	CMORPH	TAMSAT	GSMaP
HUMID	PERSIANN	ARCv2	CMORPH	TRMM	TAMSAT	GSMaP
MOIST SUB-HUMID	PERSIANN	ARCv2	TRMM	TAMSAT	CMORPH	GSMaP
DRY SUB-HUMID	PERSIANN	TRMM	ARCv2	TAMSAT	CMORPH	GSMaP
SEMI ARID	PERSIANN	TRMM	ARCv2	TAMSAT	CMORPH	GSMaP
ARID	PERSIANN	ARCv2	TRMM	CMORPH	TAMSAT	GSMaP
HYPER ARID	PERSIANN	ARCv2	TRMM	CMORPH	GSMaP	TAMSAT

a unimodal rainfall pattern, while the equatorial and southern sectors indicate a bimodal rainfall pattern with varying strengths. This unique characteristics in this subregion of Africa is linked to the movement of the ITCZ, where it moves to the north of GHA during February to May, and return to the south during October to December resulting in two rainy seasons along the equatorial region (e.g., *Beltrando and Camberlin*, 1993; *Nicholson*, 2000). These rainy seasons are, however, less intense than what is seen over western Africa due to the greater movement of the ITCZ.

GPCC and the SRS-based rainfall estimates are able to clearly reproduce the seasonal cycle very well over GHA (see, Figure 6(a-c)). However, they tend to underestimate monthly rainfall amounts in the southern sector. Gauge stations in Tanzania are mainly located along the coastal areas, where satellite-based products generally tend to underestimate surface precipitation rates (e.g., *Dinku et al.*, 2010a). While ARCv2 and GSMaP tends to underestimate rainfall in the north (Figure 6a), TAMSAT, CMORPH, and GSMaP products tend to severely underestimate rainfall over equatorial and southern sectors. TAMSAT shows the largest mean bias over

the southern sector indicating a difference of approximately 200 mm during long rain season (March-May). The scatter plots shown in Figure 6(d-f) are consistent with the seasonal rainfall pattern over the three climatic regimes. While it is obvious that TRMM and GPCC indicate the closest agreement in all the three regions, other SRS-based products also show lower biases in the upper two regions. PERSIAN, CMORPH, and GSMaP tend to show the least correlation in the southern sector, indicating that underestimations are less systematic over coastal regions. Note that 5 of the 6 rain gauges used in this study are located along the coastal regions of Tanzania.

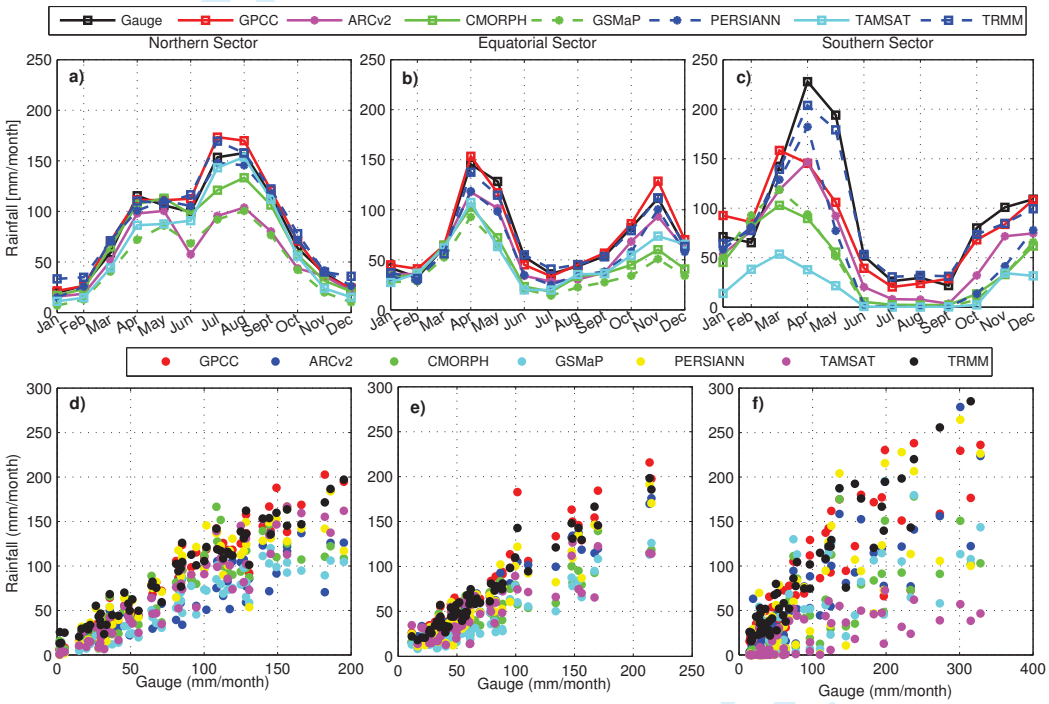

Figure 6: Comparison of various precipitation products over the GHA region with *in-situ* gauge data: (a-c) Mean seasonal cycle of rainfall over three rainfall regions of GHA for the period 2003–2007, and (d-f) scatter plots of monthly rainfall between *in-situ* observations and gridded precipitation products.

SNRs derived from RMSE values and TCH-derived noise estimates were used to rank the performances of individual gridded precipitation estimates, and the performance rankings based on RMSE and TCH-derived noise estimates undertaken in order to understand the limitations of these statistical methods. Figure 7a-d represent the MCP rankings of the gridded precipitation products over GHA. With respect to RMSE, the products are ranked in the following order: TRMM, ARCv2, CMORPH, PERSIAN, TAMSAT, and GSMaP while the TCH method ranked the noise estimates as: GSMaP, CMORPH, ARCv2, PERSIANN, TAMSAT, and TRMM. In

the context of SNRs (Figure 7 b and d) however, the products are ranked as: TRMM, ARCv2, PERSIAN, CMORPH, TAMSAT, and GSMaP; and CMORPH, GSMaP, ARCv2, PERSIANN, TRMM, and TAMSAT, for RMSE-derived and TCH-derived SNRs, respectively. Note from Figure 7, however, that many of the products are statistically similar to each other. CMORPH and GSMaP, which mainly rely on passive MW, are found effective to represent rainfall patterns over the complex terrain of GHA (*Dinku et al.*, 2007, 2008, 2010b; *Thiemig et al.*, 2012).

The comparative evaluation of the products showed that the noise level of rainfall measurements within the wetter regions of the continent are high, especially for the products that are based on microwave measurements. This agrees with the findings of *McCollum et al.* (2000) and *Habib et al.* (2012), who reported over-estimation over highly convective regions of equatorial central Africa and Guinea regions (see, e.g., *Webster*, 1983). The central African region experiences one of the most intense convections on the Earth, which is a very strong indicator of ice-hydrometeors responsible for forming precipitation. *McCollum et al.* (2000) related this inefficient rainfall formation to the physical properties of air masses and cloud structure in the region. Convective clouds under dry conditions have relative higher cloud bases forming moist environment, which leads to high evaporation of the falling rain. Other factors include possible abundance of aerosols as a result of extensive biomass burning in the region (*Ekman et al.*, 2004), resulting in high density of cloud condensation nuclei, which leads to an inefficient rain process (e.g., *McCollum et al.*, 2000; *Ekman et al.*, 2004; *Habib et al.*, 2012).

Magnitudes of noise levels in PERSIANN, compared to others in all climate zones, are found to be the lowest, while the noise estimates of GSMaP are found to be the highest (cf., Tables 3 and 4). Over the continent, ARCv2 and TAMSAT are found to be statistically similar in terms of uncertainties, followed by TRMM. Considering the SNRs, ARCv2 and TRMM represent similar quality (Table 4), consistent with the findings of *Thiemig et al.* (2012), who showed that TRMM and RFE2 (ARCv2's precursor) are similar over the continent. CMORPH is ranked above TAMSAT, which is also rated better than GSMaP. This is consistent with the findings of *Dinku et al.* (2007) and *Thiemig et al.* (2012) that the product (CMORPH) is of an appreciable performance over the continent although it is not merged with RG observations. However, its tendency to overestimate rainfall in different parts of the continent have been reported in other studies (e.g., *Dinku et al.*, 2007; *Jobard et al.*, 2011). The CMORPH algorithm, which highly relies on passive microwave data, over-estimates rainfall in Africa (see, e.g., *Nichol-*

son et al., 2003a). This is confirmed by the high amplitudes observed for the product from the CEOF results discussed in the next section. It is, therefore, possible that its overestimations yield higher SNR values. Conversely, TAMSAT's low performance, relative to CMORPH and TRMM, could be due to the lack of microwave data and post-estimation adjustments (see, e.g., *Dinku et al.*, 2007) leading to low signal amplitudes as observed in the CEOF results (see section 5.5). ARCv2 represents good performance both in noise estimates and SNRs, which can be due to the use of various (infra red (IR), microwave, and contemporaneous (RG) information.

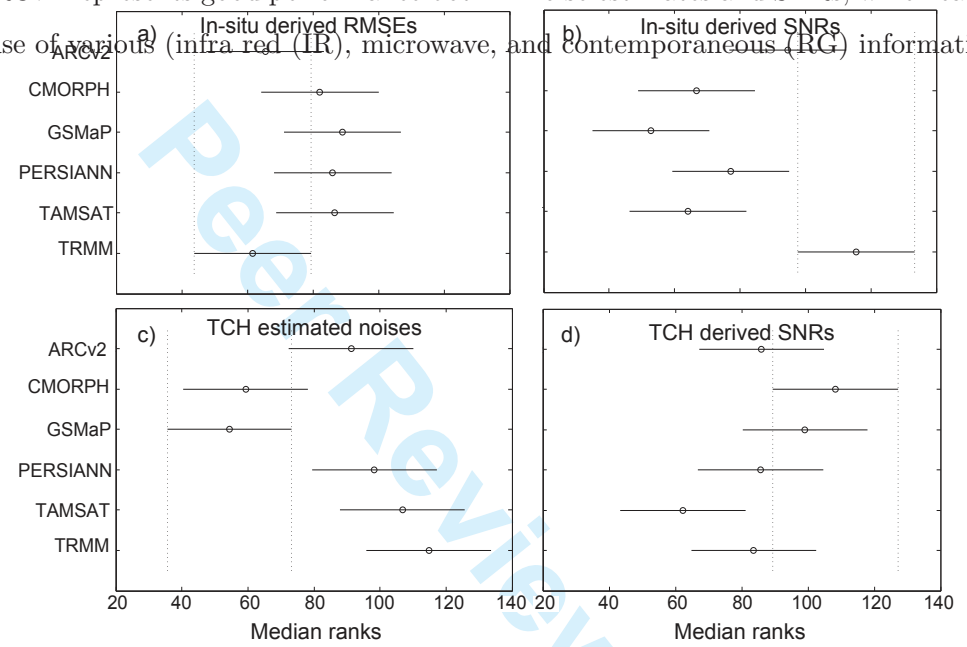

Figure 7: Performance rankings of the six SRS-based products over the GHA region based on (a) RMSEs, (b) SNRs derived from RMSE, (c) TCH-derived noise estimates, and d) SNRs derived from TCH noise estimates. The lower x-axis values in (a) and (c), and higher x-axis values in (b) and (d) indicate better performance.

5.5. Spatio-temporal variability of rainfall over Africa (2003-2010)

In order to assess the spatio-temporal behavior of rainfall variability over Africa, CEOF was applied to each individual gridded precipitation product for the period of 2003-2010. Focuss is on the first two leading CEOF modes that accounts for 85% of the rainfall variability over Africa. The temporal amplitude, spatial amplitude, and spatial phase of the first CEOF mode of all the products are shown in Figures 8, 9, and 10 respectively. The temporal phase patterns are not shown here since the temporal components are found to be cyclic, and no meaningful changes in the temporal phase evoloution were noted.

The first mode of all products accounts for more than 65% of the total variance in all the datasets, with TAMSAT having the largest variance of 72.8%. The temporal evolutions, shown

in Figure 8, indicate annual rainfall variability over the entire African continent. The first and last two months were removed after applying the Hilbert transform before the singular value decomposition of complex fields to avoid artifacts at the beginning and end of the time series. The temporal evolutions indicate high interannual variability with distinct high (e.g., 2007) and low (e.g., 2005, 2009) peaks between 2003 and 2010 in their amplitudes. Although the temporal patterns are quite similar in all the datasets, their representation of the lower peaks are not very consistent in some of the datasets (e.g., ARCv2 and CMORPH). Year to year rainfall variations derived from TAMSAT were smaller than the other products.

The amplitudes of the spatial pattern (Figure 9) indicate the maximum amount of annual rainfall over eastern Congo, western borders of Ethiopia, west coast regions of Guinea, and coastal regions of northern Madagascar. The lowest rainfall regions include the two desert regions at the two ends (Sahara and Kalahari, see Figure 1) of the African continent, which include Algeria, northern Mali and Mauritania, western borders of Somalia in the north, and southern parts of the African peninsula including South Africa, Namibia, Zimbabwe, Botswana, and Angola. The East African region of Somalia is known for its aridity and recurring droughts (*Maystadt and Ecker*, 2014), which is apparent in all the precipitation products.

From Figure 9, one can see that GPCC, TRMM, and PERSIANN indicate very similar spatial patterns while the two regional products namely ARCv2 and TAMSAT indicate equivalent magnitudes of rainfall over Africa. The satellite-only products (CMORPH and GSMaP) on the other hand, represent anomalously high rainfall over the central African region (e.g., Congo, Central African Republic) and the Guinea coast, which are known for large convective activities (*Webster*, 1983). The spatial propagation of the annual rainfall is shown in Figure 10, where each degree change in the phase value (-180 to +180°) corresponds to 1 day. Based on the results in Figures 9 and 10, maximum rainfall is observed during the boreal winter (austral summer) over the northern Africa peaking in December, while the rest of region sees maximum rainfall during the boreal summer. The movement of the rain belt as shown by the CEOF agrees with that of the ITCZ, north and south of the equator as noted by *Nicholson* (2000).

Figures 11, 12, and 13 show temporal evolutions, the spatial amplitudes, and the associated spatial phase propagations of the second CEOF mode. The second mode explains about 20% of the rainfall variability over Africa and is related to the intra-annual variability of rainfall over Africa. The second mode of various products is found to be more comparable than the

first mode.

The amplitudes of the second CEOF mode (Figure 11) indicate intra-annual changes in rainfall, which are mostly influenced by the high equatorial rainfall regime as can be detected from the spatial patterns of Figure 12. Considering Figures 11 and 12, a relatively smaller amplitude of rainfall is detected over the two ends of the African continent. The extreme rainfall events are better represented by this mode, specially those derived from ARCv2, GPCC, PERSIANN, and TRMM. For instance, several African nations have experienced extreme rainfall in 2007 starting from Southern Africa (austral summer) to the West African nations (boreal summer) (e.g., *Tschakert et al.*, 2010) causing floods and flash floods affecting more than 1.5 million people. Extreme droughts were reported especially following very weak rainfall during the long rainy months of 2009 over most of Sahel and the GHA region (see, http://earthobservatory.nasa.gov/IOTD/view.php?id=39363&eocn=image&eoci=related_image). These extreme events are well-captured by most of the products except CMORPH and TAMSAT.

The spatial amplitudes in Figure 12 depicts mainly two rainfall patterns over the entire African continent with North Africa and GHA having one pattern and the rest of the continent having the other pattern. This patterns are nonetheless similar to the spatial amplitudes in the first mode. Anomalously high rainfall patterns over West African coasts could be related to the Atlantic semi-annual dipole structure as it has been found to be highly correlated with the Atlantic ocean-atmospheric interactions (*Forootan et al.*, 2014) while similar patterns over the GHA region may be indicate the influence of the coupled ENSO (El-Niño Oscillation)-IOD (Indian Ocean Dipole) phenomena. The spatial phase (Figure 13) represents the lateral

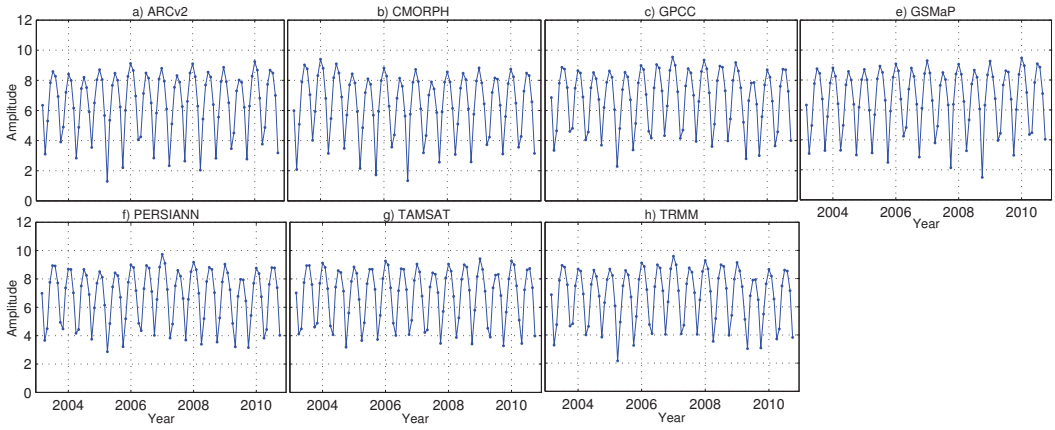

Figure 8: Temporal amplitudes derived from the first CEOF modes of various gridded precipitation estimates. This pattern represents the annual rainfall variability over Africa (the spatial amplitudes in Figure 9).

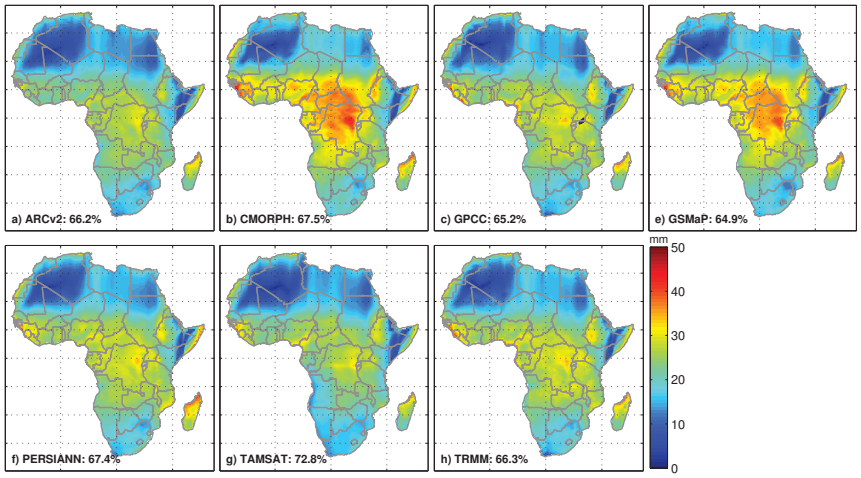

Figure 9: Spatial amplitudes of various gridded precipitation estimates for the first CEOF, corresponding to Figure 8.

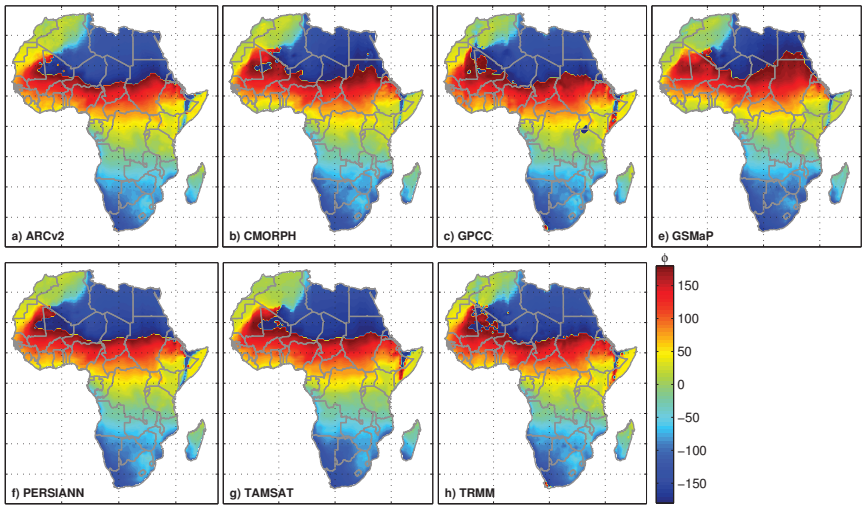

Figure 10: Spatial phases of various gridded precipitation estimates for the first CEOF describing the spatial propagation of annual rainfall over Africa. In this figure, 0° corresponds to December while -180° and 180° represents June and July, respectively.

propagation of the intra-annual signal to the equator. The phase estimations from various products are mostly similar over most parts of the continent except the coastal regions of Mauritania (West Africa) and the GHA region.

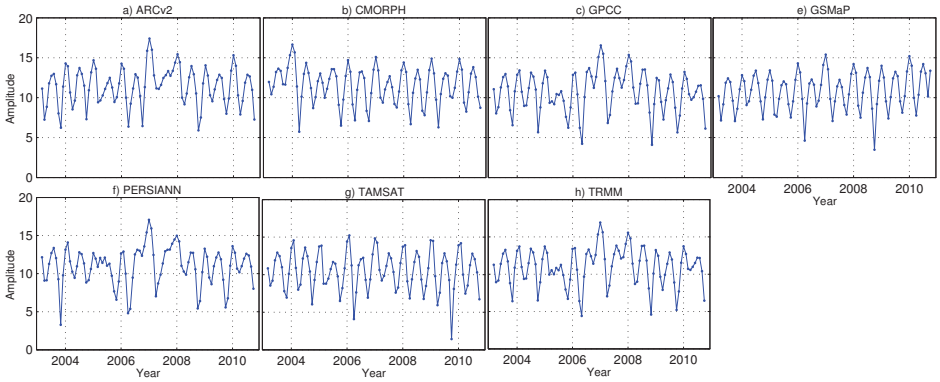

Figure 11: Temporal amplitude of the second mode of CEOF, derived from various gridded precipitation products. The patterns represent the intra-annual rainfall variability over Africa.

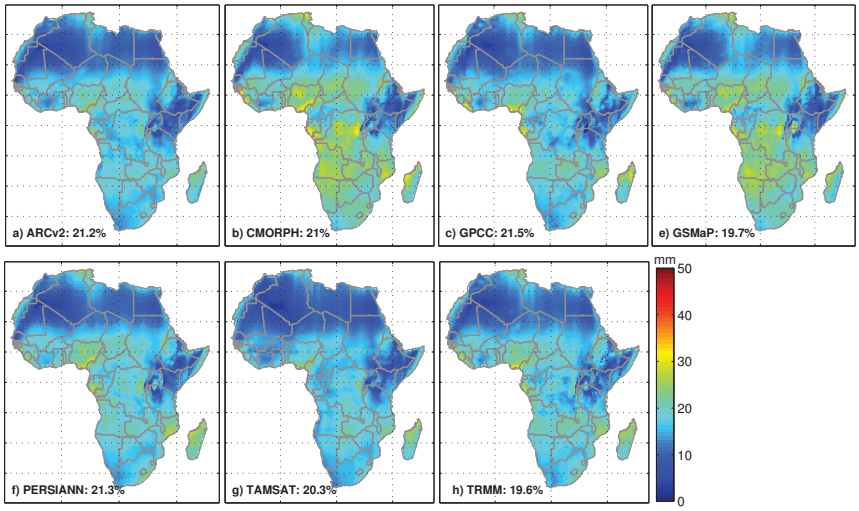

Figure 12: Spatial amplitudes of various gridded precipitation estimates for the second CEOF describing the seasonal rainfall variability over Africa.

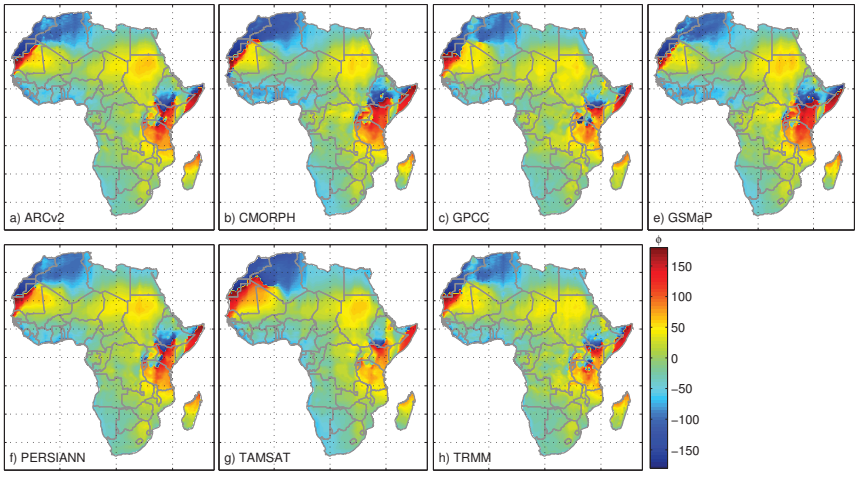

Figure 13: Spatial phases of various gridded precipitation estimates for the second CEOF describing the intra-annual rainfall variability over Africa.

The propagating patterns derived from CEOF indicate that all the products represented the annual and intra-annual variability in a similar manner. The amplitudes of CMORPH and GSMaP, however, were higher than the other products, while TAMSAT and ARCv2 had the lowest amplitudes. This agrees with the findings in Section 5.1, which showed the tendency of these data to overestimate or underestimate rainfall over the region, compare Figure 3(a-f) and Figure 9(a-g). These results also explain the higher SNRs derived from TAMSAT compared to those of GSMaP, although the former contains higher noise estimates.

5.6. Comparing TCH and the classical RG-based validation

In Section 5.1, considering the classical comparisons, the quality of TRMM was found to be better than PERSIANN and ARCv2, both in terms of noise level (i.e., RMSEs) and SNRs (cf., Table 3). A similar result is found by applying the TCH method (cf., Table 4) with the exception of TRMM. As earlier stated in Section 3, TRMM is adjusted to GPCC, therefore its closeness to GPCC is expected. The TCH method on the other hand, ranks the quality of PERSIANN, ARCv2, and TAMSAT above TRMM in terms of noise estimates, and PERSIANN and ARCv2 (above TRMM) in terms of SNRs. The noise level, found in TAMSAT, is statistically similar to that of ARCv2. However, its amplitude is lower, which provides smaller SNRs. It is worth mentioning here that, the SNR ranks of CMORPH, TAMSAT and GSMaP are largely consistent in both approaches, which proves their comparable performance.

Based on RMSEs over the GHA, the classical method shows that TRMM and ARCv2 are more consistent with gauge observations (cf., Figure 7a), whereas the TCH method ranks noise estimates of GSMaP and CMORPH as the lowest (cf., Figure 7c). Considering the fact that TRMM and ARCv2 are calibrated using GPCC and GTS, respectively, it is likely that they already contain the RG stations used in this evaluation. As such, the RMSEs are expected to be low. Considering SNRs, however, both methods show that the microwave reliant products are better suited to monitor rainfall in the region.

6. Summary of results and conclusion

Generally, from the available rainfall datasets used in this study, over the period of 2003-2010, the SRS-merged RG products are ranked high in terms of SNRs as the best over the continent from the GPCC- and TCH-based uncertainty estimations. The GPCC ranks based

on SNRs showed TRMM, PERSIANN and ARCv2 as the best products over Africa, while TCH classified PERSIANN, ARCv2 and TRMM as the best rainfall estimations. Furthermore, the efficiency of GPCC and TCH in determining the quality of SRS-rainfall products is evident in the evaluation of SRS-only rainfall products (i.e., CMORPH, TAMSAT and GSMaP) as shown in Tables 3 and 4, respectively. Table 5 presents a summary of the previous results on validation of rainfall products over Africa and/or various climate regions. Continent wide, *Novella and Thiaw* (2013) validated the ARCv2, TRMM-3B42 (version 6), and CMORPH with independent gauge data, and found RMSEs of 11.3, 13.4, and 14.0 mm/day, respectively. Despite the differences in the temporal resolution and the TRMM version, the findings in *Novella and Thiaw* (2013) are comparable to those of Table 4.

[TABLE 5 AROUND HERE.]

Overall, the results reported by *Dinku et al.* (2008) and *Romilly and Gebremichael* (2011) indicated that the CMORPH and TRMM-3B42 are better suited than PERSIANN over Ethiopia. These are somewhat comparable with the results presented in Figure 7d, where TCH derived SNRs ranked CMORPH as the best product over GHA. From Figure 7d, one can also see the overlapping whiskers of TRMM and PERSIANN that is interpreted here as their statistical similarity. However, the *in-situ* derived SNRs ranked TRMM better than PERSIANN and CMORPH. Despite the degree of similarity between PERSIANN and CMORPH, in terms of RMSE, that of CMORPH is found slightly lower than PERSIANN (Figure 7a). Additionally, considering the SRS-only products (i.e., CMORPH and GSMaP) *in-situ* and TCH based SNRs ranking, CMORPH was found to be better than GSMaP over GHA (Figure 7 b and d). These findings are consistent with *Dinku et al.* (2007), who reported CMORPH to be the best rainfall estimation over the Eastern Africa, which exhibits a complex topography. Their result also indicated that rainfall estimation from CMORPH is more reliable than TAMSAT, which seems to be confirmed by the rankings presented in Figure 7 (b and d).

Overall, considering the results of TCH over the 2003-2010 study period, (i) PERSIANN product are found to be reliable product over the African continent, while the GPCC-based validation ranked TRMM as the best. However, considering both GPCC- and TCH-based evaluation methods, relatively lower quality in GSMaP, TAMSAT and CMORPH (sorted in a descending order) were found. (ii) TRMM and ARCv2, are found to be statistically similar and are ranked after PERSIANN based on the TCH method. (iii) Over GHA, SNRs derived from

both methods ranked CMORPH and GSMaP as the best performing products, while TAMSAT and TRMM were ranked the least, although most of the datasets were found to be statistically similar.

The CEOF results indicated that all the evaluated products exhibit similar spatio-temporal patterns over the continent. TAMSAT estimates showed smaller annual and semi-annual amplitudes over the continent, while those of CMORPH were found to be higher, both in agreement with the GPCC-based validation. TAMSAT's low amplitudes could be related to the dry biases, which affect its general performance in representing rainfall variability despite its relatively low noise estimates. It is worth noting that the reported results obtained are valid for the SRS products used for this study between 2003 and 2010 over the whole continent, as well as its major climatic zones. Different results could be obtained within different time frames as well as geographical locations, as exhibited in the validation over GHA. Further studies, which take a new version of TAMSAT (*Tarnavsky et al.*, 2014) into account, will need to be performed. For overall applications, the findings of this study supports the choice of SRS-based precipitation products enhanced by ground observations.

Acknowledgments

V. G. Ferreira was partially supported by the National Natural Science Foundation of China (Grant No. 41204016). We would like to express our sincere gratitude to the IGAD's Climate Prediction and Application Center (ICPAC) for providing the *in-situ* gauge observations. We are also grateful to the providers of the following rainfall products: Global Precipitation Climatology Centre (GPCC), African Rainfall Climatology Version 2 (ARCv2), Climate Prediction Center (CPC) Morphing Technique (CMORPH), Global Satellite Mapping of Precipitation moving vector with Kalman filter (GSMaP-MVK), Precipitation Estimation from Remotely Sensed Information using Artificial Neural Networks (PERSIANN), Tropical Applications of Meteorology using Satellite data and ground-based observations (TAMSAT), and Tropical Rainfall Measuring Mission (TRMM). We thank Prof. Radan Huth (Editor-in-Chief) and the two anonymous reviewers for their constructive comments that helped us to improve the quality of this manuscript. This work is a TIGeR publication No. 590.

References

Adeyewa, Z. D., and K. Nakamura (2003), Validation of TRMM radar rainfall data over major climatic regions in africa, *Journal of Applied Meteorology*, *42*(2), 331–347, doi: 10.1175/1520-0450(2003)042⟨0331:VOTRRD⟩2.0.CO;2.

Awange, J. L., R. Anyah, N. Agola, E. Forootan, and P. Omondi (2013), Potential impacts of climate and environmental change on the stored water of lake victoria basin and economic implications, *Water Resource Research*, *49*, 8160–8173, doi:10.1002/2013WR014350.

Awange, J. L., E. Forootan, K. Fleming, and G. Odhiambo (2014a), Dominant patterns of water storage changes in the nile basin during 2003–2013, *Remote Sensing of the Terrestrial Water Cycle*, pp. 367–381.

Awange, J. L., E. Forootan, M. Kuhn, J. Kusche, and B. Heck (2014b), Water storage changes and climate variability within the nile basin between 2002 and 2011, *Advances in Water Resources*, *73*, 1–15, doi:http://dx.doi.org/10.1016/j.advwatres.2014.06.010.

Awange, J. L., M. Gebremichael, E. Forootan, G. Wakbulcho, R. Anyah, V. G. Ferreira, and T. Alemayehu (2014c), Characterization of ethiopian mega hydrogeological regimes using grace, trmm and gldas datasets, *Advances in Water Resources*, *73*, 64–78, doi:http://dx.doi.org/10.1016/j.advwatres.2014.07.012.

Becker, A., P. Finger, A. Meyer-Christoffer, B. Rudolf, K. Schamm, U. Schneider, and M. Ziese (2013), A description of the global land-surface precipitation data products of the Global Precipitation Climatology Centre with sample applications including centennial (trend) analysis from 1901present, *Earth Syst. Sci. Data*, *5*(1), 71–99, doi:10.5194/essd-5-71-2013.

Beltrando, G., and P. Camberlin (1993), Interannual variability of rainfall in the eastern horn of Africa and indicators of atmospheric circulation, *International Journal of Climatology*, *13*(5), 533546, doi:10.1002/joc.3370130505.

Bowden, J. H., and F. H. M. Semazzi (2007), Empirical analysis of intraseasonal climate variability over the greater horn of africa, *Journal of Climate*, *20*, 57155731, doi: 10.1175/2007JCLI1587.1.

Cattani, E., A. Merino Suances, and V. Levizzani (2014), Evaluation of six satellite rainfall products over the great horn of africa, in *EGU General Assembly Conference Abstracts*, vol. 16, p. 12450.

Conti, F. L., K.-L. Hsu, L. V. Noto, and S. Sorooshian (2014), Evaluation and comparison of satellite precipitation estimates with reference to a local area in the mediterranean sea, *Atmospheric Research*, *138*(0), 189–204, doi:http://dx.doi.org/10.1016/j.atmosres.2013.11.011.

Conway, D., A. Persechino, S. Ardoin-Bardin, H. Hamandawana, C. Dieulin, and G. Mahé (2009), Rainfall and Water Resources Variability in Sub-Saharan Africa during the Twentieth Century, *Journal of Hydrometeorology*, *10*(1), 41–59, doi:10.1175/2008JHM1004.1.

Cromwell, D. (2006), Temporal and spatial characteristics of sea surface height variability in the North Atlantic Ocean, *Ocean Science Discussions*, *3*(3), 609–636, doi:10.5194/osd-3-609-2006.

Day, R. W., and G. P. Quinn (1989), Comparisons of treatments after an analysis of variance in ecology, *Ecological Monographs*, *59*(4), 433–463, doi:10.2307/1943075.

Dinku, T., P. Ceccato, E. Grover-Kopec, M. Lemma, S. J. Connor, and C. F. Ropelewski (2007), Validation of satellite rainfall products over East Africa's complex topography, *International Journal of Remote Sensing*, *8*(7), 1503–1526, doi:10.1080/01431160600954688.

Dinku, T., S. Chidzambwa, P. Ceccato, S. J. Connor, and C. F. Ropelewski (2008), Validation of high-resolution satellite rainfall products over complex terrain, *International Journal of Remote Sensing*, *29*(14), 4097–4110, doi:10.1080/01431160701772526.

Dinku, T., P. Ceccato, K. Cressman, and S. J. Connor (2010a), Evaluating detection skills of satellite rainfall estimates over desert locust recession regions, *J. Appl. Meteor. Climatol.*, *49*, 13221332.

Dinku, T., S. Connor, and P. Ceccato (2010b), Comparison of cmorph and trmm-3b42 over mountainous regions of africa and south america, in *Satellite Rainfall Applications for Surface Hydrology*, edited by M. Gebremichael and F. Hossain, pp. 193–204, Springer Netherlands, doi:10.1007/978-90-481-2915-7_11.

Dinku, T., S. Connor, and P. Ceccato (2011), *Nile River Basin- Hydrology, Climate and Water Use*, chap. Evaluation of Satellite Rainfall Estimates and Gridded Gauge Products over the Upper Blue Nile Region, pp. 109–127, Springer Netherlands, doi:10.1007/978-94-007-0689-7_5.

Ekman, A. M. L., C. Wang, J. Wilson, and J. Ström (2004), Explicit simulations of aerosol physics in a cloud-resolving model: a sensitivity study based on an observed convective cloud, *Atmospheric Chemistry and Physics*, *4*(3), 773–791, doi:10.5194/acp-4-773-2004.

Forootan, E. (2014), Statistical signal decomposition techniques for analyzing time-variable satellite gravimetry data, Ph.D. thesis, University of Bonn, Germany.

Forootan, E., J. Kusche, I. Loth, W.-D. Schuh, A. Eicker, J. Awange, L. Longuevergne, B. Diekkrüger, M. Schmidt, and C. Shum (2014), Multivariate prediction of total water storage changes over west africa from multi-satellite data, *Surveys in Geophysics*, pp. 1–28, doi:10.1007/s10712-014-9292-0.

Funk, C., and J. Verdin (2003), Comparing satellite rainfall estimates and reanalysis precipitation fields with station data for Western Kenya, in *JRC-FAO International Workshop on Crop and Rangeland Monitoring in Eastern Africa for Early Warning and Food Security in Africa*, p. 8996, European Commission and FAO: Ispra, Nairobi, 2830 January 2003.

Galindo, F. J., and J. Palacio (1999), Estimating the instabilities of N correlated clocks, in *Proceedings of the 31st Annual Precise Time and Time Interval (PTTI) Meeting*, pp. 285–296, Dana Point, California.

Galindo, F. J., and J. Palacio (2003), Post-processing ROA data clocks for optimal stability in the ensemble timescale, *Metrologia*, *40*(3), S237–S244, doi:10.1088/0026-1394/40/3/301.

Giesen, N. V. D., J. Liebe, and G. Jung (2010), Adapting to Climate Change in the Volta Basin, West Africa, *Current Science*, *98*(8), 1033 – 1037.

Gray, J. E., and D. W. Allan (1974), A method for estimating the frequency stability of an individual oscillator, in *Proc 8th Ann. Symp. on Frequency Control*, vol. 2439, pp. 277–287.

Grimes, D., E. Pardo-Igúzquiza, and R. Bonifacio (1999), Optimal areal rainfall estimation using raingauges and satellite data, *Journal of Hydrology*, *222*(1-4), 93–108, doi:10.1016/S0022-1694(99)00092-X.

Habib, E., M. ElSaadani, and A. T. Haile (2012), Climatology-Focused evaluation of CMORPH and TMPA satellite rainfall products over the Nile basin, *J. Appl. Meteor. Climatol.*, *51*, 21052121.

Haile, A. T., E. Habib, M. Elsaadani, and T. Rientjes (2012), Inter-comparison of satellite rainfall products for representing rainfall diurnal cycle over the Nile basin, *International Journal of Applied Earth Observation and Geoinformation*, *21*, 230240.

Hsu, K.-L., and S. Sorooshian (2008), Satellite-based precipitation measurement using persiann system, in *Hydrological Modelling and the Water Cycle*, *Water Science and Technology Library*, vol. 63, edited by S. Sorooshian, K.-L. Hsu, E. Coppola, B. Tomassetti, M. Verdecchia, and G. Visconti, pp. 27–48, Springer Berlin Heidelberg, doi:10.1007/978-3-540-77843-1_2.

Huffman, G. J., D. T. Bolvin, E. J. Nelkin, D. B. Wolff, R. F. Adler, G. Gu, Y. Hong, K. P. Bowman, and E. F. Stocker (2007), The TRMM Multisatellite Precipitation Analysis (TMPA): Quasi-Global, Multiyear, Combined-Sensor Precipitation Estimates at Fine Scales, *Journal of Hydrometeorology*, *8*(1), 3855, doi:10.1175/JHM560.1.

Huffman, G. J., R. F. Adler, D. T. Bolvin, and E. J. Nelkin (2010), The TRMM Multi-Satellite Precipitation Analysis (TMPA), in *Satellite Rainfall Applications for Surface Hydrology*, edited by M. Gebremichael and F. Hossain, pp. 3–22, Springer Netherlands, doi:10.1007/978-90-481-2915-7_1.

Hughes, D. (2006), Comparison of satellite rainfall data with observations from gauging station networks, *Journal of Hydrology*, *327*(3-4), 399–410, doi:10.1016/j.jhydrol.2005.11.041.

Janowiak, J., A. Gruber, C. R. Kondragunta, R. E. Livezey, and G. J. Huffman (1998), A comparison of the NCEP-NCAR reanalysis precipitation and the GPCP rain gauge-satellite combined dataset with observational error considerations, *Journal of Climate*, *11*, 2960–2979.

Jobard, I., F. Chopin, J. C. Berges, and R. Roca (2011), An intercomparison of 10-day satellite precipitation products during West African monsoon, *International Journal of Remote Sensing*, *32*(9), 2353–2376, doi:10.1080/01431161003698286.

Joyce, R. J., J. E. Janowiak, P. A. Arkin, and P. Xie (2004), CMORPH: A method that produces global precipitation estimates from passive microwave and infrared data at high spatial and temporal resolution, *Journal of Hydrometeorology*, *5*, 487–503.

Kidd, C., P. Bauer, J. Turk, G. J. Huffman, R. Joyce, K.-L. Hsu, and D. Braithwaite (2012), Intercomparison of high-resolution precipitation products over northwest europe, *Journal of Hydrometeorology*, *13*(1), 67–83, doi:10.1175/JHM-D-11-042.1.

Koot, L., O. D. Viron, and V. Dehant (2006), Atmospheric angular momentum time-series: Characterization of their internal noise and creation of a combined series, *Journal of Geodesy*, *79*(12), 663674, doi:10.1007/s00190-005-0019-3.

Kummerow, C., W. Barnes, T. Kozu, J. Shiue, and J. Simpson (1998), The Tropical Rainfall Measuring Mission (TRMM) Sensor Package, *Journal of Atmospheric and Oceanic Technology*, *15*, 809817, doi:10.1175/1520-0426(1998)015⟨0809:TTRMMT⟩2.0.CO;2.

Kummerow, C., P. Poyner, W. Berg, and J. Thomas-Stahle (2004), The effects of rainfall inhomogeneity on climate variability of rainfall estimated from passive microwave sensors, *J. Atmos. Oceanic Technol.*, *21*, 624638.

Li, L., Y. Hong, J. Wang, R. Adler, F. Policelli, S. Habib, D. Irwn, T. Korme, and L. Okello (2009), Evaluation of the real-time TRMM-based multi-satellite precipitation analysis for an operational flood prediction system in Nzoia Basin, Lake Victoria, Africa, *Natural Hazards*, *50*(1), 109–123, doi:10.1007/s11069-008-9324-5.

Liechti, T. C., J. P. Matos, J. L. Boillat, and A. J. Schleiss (2012), Empirical analysis of intraseasonal climate variability over the Greater Horn of Africa, *Hydrol. Earth Syst. Sci.*, *16*, 489–500, doi:10.5194/hess-16-489-2012.

Maidment, R. I., D. I. F. Grimes, R. P. Allan, H. Greatrex, O. Rojas, and O. Leo (2013), Evaluation of satellite-based and model re-analysis rainfall estimates for Uganda, *Meteorological Applications*, *20*(3), 308–317, doi:10.1002/met.1283.

Maystadt, J.-F., and O. Ecker (2014), Extreme weather and civil war: Does drought fuel conflict in somalia through livestock price shocks?, *American Journal of Agricultural Economics*, pp. Published electronically March 25, 2014, doi:10.1093/ajae/aau010.

McCollum, J. R., A. Gruber, and M. B. Ba (2000), Discrepancy between gauges and satellite estimates of rainfall in Equatorial Africa, *Journal of Applied Meteorology*, *39*(5), 666–679, doi:10.1175/1520-0450-39.5.666.

McKight, P. E., and J. Najab (2010), *Kruskal–Wallis Test*, John Wiley & Sons, Inc., doi: 10.1002/9780470479216.corpsy0491.

Nesbitt, S. W., D. J. Gochis, and T. J. Lang (2008), The diurnal cycle of clouds and precipitation along the sierra madre occidental observed during name-2004: Implications for warm season precipitation estimation in complex terrain, *Journal of Hydrometeorology*, *9*(4), 728–743, doi:10.1175/2008JHM939.1.

Nicholson, S. E. (1986), The Spatial Coherence of African Rainfall Anomalies: Interhemispheric Teleconnections, *J. Climate Appl. Meteor.*, *25*(10), 1365–1381, doi:http://dx.doi.org/10.1175/1520-0450(1986)025⟨1365:TSCOAR⟩2.0.CO;2.

Nicholson, S. E. (2000), The nature of rainfall variability over Africa on time scales of decades to millenia, *Global and Planetary Change*, *26*(1-3), 137158, doi:10.1016/S0921-8181(00)00040-0.

Nicholson, S. E. (2013), The West African Sahel: A Review of Recent Studies on the Rainfall Regime and Its Interannual Variability, *ISRN Meteorology*, *2013*, 1–32, doi:10.1155/2013/453521.

Nicholson, S. E., B. Some, J. McCollum, E. Nelkin, D. Klotter, Y. Berte, B. M. Diallo, I. Gaye, G. Kpabeba, O. Ndiaye, J. N. Noukpozounkou, M. M. Tanu, A. Thiam, A. A. Toure, and A. K. Traor (2003a), Validation of TRMM and other rainfall estimates with a high-density gauge dataset for West Africa. Part I: Validation of GPCC rainfall product and pre-TRMM satellite and blended products, *Journal of Applied Meteorology*, *42*(10), 1337–1354, doi:10.1175/1520-0450(2003)042⟨1337:VOTAOR⟩2.0.CO;2.

Nicholson, S. E., B. Some, J. McCollum, E. Nelkin, D. Klotter, Y. Berte, B. M. Diallo, I. Gaye, G. Kpabeba, O. Ndiaye, J. N. Noukpozounkou, M. M. Tanu, A. Thiam, A. A. Toure, and A. K. Traor (2003b), Validation of TRMM and other rainfall estimates with a high-density gauge dataset for West Africa. Part II: Validation of TRMM rainfall products, *Journal of Applied Meteorology*, *42*(10), 1355–1368, doi:10.1175/1520-0450(2003)042⟨1355:VOTAOR⟩2.0.CO;2.

Novella, N. S., and W. M. Thiaw (2013), African Rainfall Climatology Version 2 for famine early warning systems, *Journal of Applied Meteorology and Climatology*, *52*, 588606, doi: 10.1175/JAMC-D-11-0238.1.

Omondi, P. A., J. L. Awange, L. Ogallo, R. Okoola, and E. Forootan (2012), Decadal rainfall variability modes in observed rainfall records over east africa and their relations to historical sea surface temperature changes, *Journal of Hydrology*, *464-465*, doi:dx.doi.org/10.1016/j.jhydrol.2012.07.003.

Omondi, P. A., J. L. Awange, L. A. Ogallo, J. Ininda, and E. Forootan (2013), The influence of low frequency sea surface temperature modes on delineated decadal rainfall zones in eastern africa region, *Advances in Water Resources*, *54*, doi:dx.doi.org/10.1016/j.advwatres.2013.01.001.

Omondi, P. A., J. L. J. Awange, E. Forootan, L. A. Ogallo, R. Barakiza, G. B. Girmaw, I. Fesseha, V. Kululetera, C. Kilembe, M. M. Mbati, M. Kilavi, S. M. King'uyu, P. A. Omeny, A. Njogu, E. M. Badr, T. A. Musa, P. Muchiri, D. Bamanya, and E. Komutunga (2014), Changes in temperature and precipitation extremes over the greater horn of africa region from 1961 to 2010, *International Journal of Climatology*, *34*(4), 1262–1277, doi:10.1002/joc.3763.

Preisendorfer, R. W. (1988), *Principal component analysis in meteorology and oceanography*, 436 pp., Elsevier, Amsterdam.

Rafter, J., M. Abell, and J. Braselton (2002), Multiple comparison methods for means, *SIAM Review*, *44*(2), 259–278, doi:10.1137/S0036144501357233.

Rojas, O., A. Vrieling, and F. Rembold (2011), Assessing drought probability for agricultural areas in Africa with coarse resolution remote sensing imagery, *Remote Sensing of Environment*, *115*(2), 343–352, doi:10.1016/j.rse.2010.09.006.

Romilly, T. G., and M. Gebremichael (2011), Evaluation of satellite rainfall estimates over Ethiopian river basins, *Hydrol. Earth Syst. Sci.*, *15*, 1505–1514, doi:10.5194/hess-15-1505-2011.

Sawunyama, T., and D. A. Hughes (2008), Application of satellite-derived rainfall estimates to extend water resource simulation modelling in South Africa, *Water SA*, *34*(1), 1–9.

Schneider, U., A. Becker, P. Finger, A. Meyer-Christoffer, M. Ziese, and B. Rudolf (2013), GPCC's new land surface precipitation climatology based on quality-controlled in situ data and its role in quantifying the global water cycle, *Theor Appl Climatol*, pp. 15–40, doi:10.1007/s00704-013-0860-x.

Seo, K.-W., C. R. Wilson, J. S. Famiglietti, J. L. Chen, and M. Rodell (2006), Terrestrial water mass load changes from gravity recovery and climate experiment (grace), *Water Resources Research*, *42*(5), n/a–n/a, doi:10.1029/2005WR004255.

Smith, T. M., P. A. Arkin, J. J. Bates, and G. J. Huffman (2006), Estimating bias of satellite-based precipitation estimates, *Journal of Hydrometeorology*, *7*(5), 841–856, doi: 10.1175/JHM524.1.

Sorooshian, S., K.-L. Hsu, X. Gao, H. V. Gupta, B. Imam, and D. Braithwaite (2000), Evaluation of PERSIANN System satellitebased estimates of tropical rainfall, *Bulletin of the American Meteorological Society*, *81*(9), 2035–2046, doi:10.1175/1520-0477(2000)081⟨2035: EOPSSE⟩2.3.CO;2.

Tarnavsky, E., D. Grimes, R. Maidment, E. Black, R. P. Allan, M. Stringer, R. Chadwick, and F. Kayitakire (2014), Extension of the TAMSAT Satellite-based Rainfall Monitoring over Africa and from 1983 to present, *Journal of Applied Meteorology and Climatology*, doi: 10.1175/JAMC-D-14-0016.1, e-View.

Tavella, P., and A. Premoli (1994), Estimating the instabilities of n clocks by measuring differences of their readings, *Metrologia*, *30*(5), 479, doi:10.1088/0026-1394/30/5/003.

Thiemig, V., R. Rojas, M. Zambrano-Bigiarini, V. Levizzani, and A. de Roo (2012), Validation of satellite-based precipitation products over sparsely gauged African River basins, *Journal of Hydrometeorology*, *13*(6), 1760–1783, doi:10.1175/JHM-D-12-032.1.

Tschakert, P., R. Sagoe, G. Ofori-Darko, and S. Codjoe (2010), Floods in the Sahel: an analysis of anomalies, memory, and anticipatory learning, *Climatic Change*, *103*(3-4), 471–502, doi: 10.1007/s10584-009-9776-y.

Ushio, T., and M. Kachi (2010), Kalman filtering applications for global satellite mapping of precipitation (gsmap), in *Satellite Rainfall Applications for Surface Hydrology*, edited by M. Gebremichael and F. Hossain, pp. 105–123, Springer Netherlands, doi:10.1007/ 978-90-481-2915-7_7.

Wamukonya, N., B. Masumbuko, E. Gowa, and J. Asamoah (2006), Environmental State-and-Trends: 20-Year Retrospective, in *Africa Environment Outlook 2: Our Environment, Our*

Wealth, edited by J. C. Mohamed-Katerere and M. Sabet, chap. Atmosphere, pp. 48–50, DEWA/UNEP, Nairobi, Kenya.

Webster, P. J. (1983), Large-scale structure of the tropical atmosphere, in *Large-Scale Dynamical Processes in the Atmosphere*, edited by B. Hoskins and R. Pearce, pp. 235–275, Academic Press, New York.

Xie, P., and P. A. Arkin (1997), Global Precipitation: A 17-Year Monthly Analysis Based on Gauge Observations, Satellite Estimates, and Numerical Model Outputs, *Bull. Amer. Meteor. Soc.*, *78*(11), 2539–2558.

Xie, P., R. J. Joyce, and S. Wu (2015), Climate data record for high-resolution global precipitation, pp. 3414–3416, 25^{th} IGARSS Proceedings.

Table 5: Summary of previous works on validation of SRS-based rainfall products over Africa and its regions.

Products Evaluated	Region	Main Results
GPCP, GPCC, GPI, and SSM/I	West Africa	GPCC and GPCP show good agreement with gauge data, GPI and SSM/I on the other hand perform poorly (*Nicholson et al.*, 2003a).
TRMM-merged product, TRMM-AGPI, and TRMM satellite only products	West Africa	TRMM-AGPI shows a bias of 0.2 mm/day while TRMM-merged products shows small or no bias and the satellite only products tended to overestimate (*Nicholson et al.*, 2003b).
Used GPCC to validate TRMM-PR, TRMM-3B43, and GPCP-TMPI	Major climatic regions over Africa	TRMM-3B43 and GPCP-TMPI present superior performance relative to TRMM-PR (*Adeyewa and Nakamura*, 2003).
Group I: CMAP, GPCP-MS, GPCP-SG, and TRMM-3B43. Group II: TAMSAT, CMORPH, TRMM-3B42, RFE 1 & 2, ARC, and GPCP-1DD	Ethiopia (complex topography)	Group I (descending order of accuracy): CMAP, TRMM-3B43, GPCP-SG, and GPCP-MS; Group II: CMORPH, TAMSAT, TRMM-3B42, RFE 1, REF 2, ARC and and GPCP-1DD (*Dinku et al.*, 2007).
PERSIANN, CMORPH, TRMM-3B42, TRMM-3B42RT, RFE, and NRLB	Zimbabwe and Ethiopian highlands	Over Ethiopia CMORPH and TRMM-3B42 showed good performance while RFE and PERSIANN were relatively poor and RFE1 outperformed RFE2 while over Zimbabwe RFE2 and TRMM-3B42 showed good performance whereas PERSIANN had the worst performancea and RFE2 outperformed RFE1 (*Dinku et al.*, 2008).
CMORPH, PERSIANN, GPCP-1DD, GSMaP-MVK, TRMM-3B42, TRMM-3B42RT, EPSAT-SG, RFE2, TAMSAT, and GPI	West Africa (during the monsoon period)	CMORPH, PERSIANN and TRMM 3B42RT present low performance, they were all outperformed by GPI (*Jobard et al.*, 2011).
CMORPH, PERSIANN, and TRMM-3B42RT	Ethiopian river basins	CMORPH and TRMM-3B42 outperform PERSIANN (PERSIANN underestimates by 43%; CMORPH by 11% and TRMM-3B42 by 5%). TRMM-3B42 and CMORPH tend to overestimate at low elevations while they give good results at high elevations. Converse is true for PERSIANN (*Romilly and Gebremichael*, 2011).
CMORPH, PERSIANN, GSMaP-MVK, TRMM-3B42, GPROF 6.0, RFE2, and ERA-Interim	Zambezi, Volta, Juba-Shabelle, and Baro-Akobo River basins, respectively, in Southern, West and East Africa	RFE2 and TRMM-3B42 are the most accurate while GSMaP-MVK and GPROF 6.0 are the least accurate while CMORPH showed strength in the mountainous regions whereas PERSIANN had large monthly overestimation over Volta and Zambezi (*Thiemig et al.*, 2012).
ARCv2, TRMM-3B42 (version 6), and CMORPH	African continent	Overall, gauge-based validation indicates RMSEs of 11.3, 13.4 and 14 mm/day, respectively for ARCv2, TRMM-3B42 and CMORPH for the West African summer season. Slightly lower performance compared to CMORPH and TRMM-3B42 in orographic area (*Novella and Thiaw*, 2013).
TAMSAT, GSMaP, CMORPH, PERSIANN, RFE, and TRMM-3B42 validated with GPCC	GHA	TRMM-3B42, best performing product followed by TAMSAT and RFE. PERSIANN and GSMaP show the worst performance while CMORPH yielded good results over central Ethiopia (*Cattani et al.*, 2014).